ACS OMEGA

Open Access

http://pubs.acs.org/journal/acsodf

Article

Metal–Metalloid Modified C_{36} Fullerene: A Dual Role in Drug Delivery and Sensing for Anticancer Chlormethine Explored through DFT and MD Simulations

Sourav Kanti Jana, Namrata A. Tukadiya, Adisak Boonchun,* and Prafulla K. Jha*

Cite This: *ACS Omega* 2024, 9, 49786–49803

Read Online

ACCESS | Metrics & More | Article Recommendations | Supporting Information

ABSTRACT: Spurred by the latest developments and growing utilization of zero-dimensional (0D) drug delivery and drug sensors, this investigation examines the possibilities of the 0D C_{36} fullerene for drug delivery and the detection of the anticancer drug chlormethine (CHL), the overabundance of which poses a significant threat to living organisms. This study employs density functional theory and ab initio molecular dynamics (AIMD) simulations (AIMD) to evaluate and gain insights into the interaction mechanisms between pristine C_{36} fullerene, metal–metalloid (MM)-modified C_{36} fullerene (with Al, Fe, and B), and the anticancer drug CHL. It is observed that in the gas phase, the CHL drug molecule adsorbs onto the fullerenes in the following order: $B-C_{36}$ > $Fe-C_{36}$ > $Al-C_{36}$ > C_{36}. However, when considering the solvent effect, the adsorption energy of the CHL drug molecule on $B-C_{36}$ increases, indicating chemisorption behavior. This implies that $B-C_{36}$ could be a promising candidate for drug delivery applications, particularly for the CHL anticancer drug. In contrast, the adsorption energy of the CHL drug molecule on $Fe-C_{36}$ decreases with the presence of the solvent, resulting in intermediate physisorption. Due to its minimal recovery time, excellent sensing response, intermediate physisorption, and shorter interatomic distance compared to C_{36} and $Al-C_{36}$ fullerenes, $Fe-C_{36}$ is well-suited as a drug sensor for CHL. AIMD simulations demonstrate that the $B-C_{36}$/CHL and $Fe-C_{36}$/CHL complexes are well-equilibrated and highly stable in the aqueous phase at 300 and 310 K respectively, with no evidence of bond breakage or formation. The structural stability observed, even with temperature fluctuations, indicates that the electrostatic interactions are robust enough to maintain cohesion of the fragments.

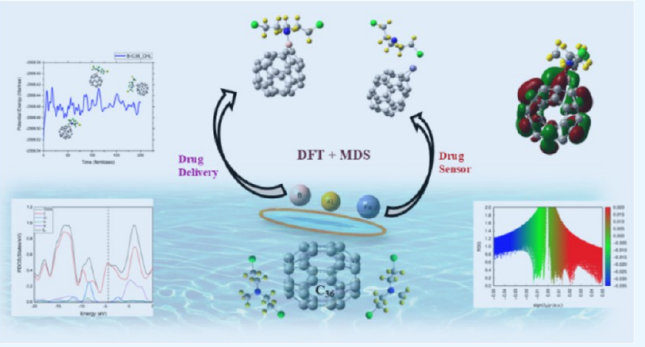

1. INTRODUCTION

Fullerenes are highly valued in scientific research, not just for their striking appearance but also for their extraordinary properties. Their distinctive capacity to act as electron acceptors in both solid and liquid states distinguishes them.[1] Following the macroscopic-scale C_{60} synthesis discovered by Kroto, attention swiftly shifted toward developing functional systems with a view to potential applications.[2] Various fullerene derivatives have exhibited a range of physical properties that make them attractive for applications in material science,[3] pharmaceuticals,[4] and biological research.[5] Their distinct hydrophobic nature allows them to dissolve more easily in organic solvents than that in polar solvents. This property is beneficial for maintaining excellent electrochemical behavior with biomolecules, along with high electron affinity and ionization potential for interactions.[6] Additionally, fullerenes have been successfully utilized as electrochemical nano sensors due to their biocompatibility, high-surface area from their spherical shape, and lower toxicity to living microorganisms compared to graphene and carbon nanotubes (CNTs).[7−10] Numerous theoretical studies have been conducted on fullerene isomers such as C_{20}, C_{24}, C_{60}, and C_{70}, predicting their significant utility in biological applications. These include biosensing,[11,12] drug delivery,[13] drug sensing,[14] and antibacterial activity,[15] among others, in recent research. In our earlier theoretical research, we identified C_{24} fullerene as a promising candidate for both biosensing and drug sensing applications.[5,16,17] In a separate study, we investigated the interaction of C_{24}, C_{36}, C_{50}, and C_{70} fullerenes with the amino acid L-leucine using both density functional theory (DFT) and classical MD simulations.[18] We found that the smaller fullerenes exhibit better binding energy with L-leucine. Building on this, we observed that the experimentally synthesized non-IPR C_{36} (D_{6h}) fullerene demonstrates a particularly intriguing interaction with the biomolecule in an aqueous environment.

Received: September 16, 2024
Revised: November 19, 2024
Accepted: November 22, 2024
Published: December 2, 2024

Its interaction energy significantly increased compared with the other fullerenes, attributed to its lower band gap relative to C_{24}, C_{50}, and C_{70}. Furthermore, C_{36} fullerene has garnered significant scientific attention due to its fused five-membered rings, which create substantial strain and increase its reactivity.[19,20] Reina et al. also suggested that C_{36} fullerene holds promise as a nano vehicle for delivering neuroprotective drugs.[21]

Rising concerns about counterfeit pharmaceutical products and the questionable practices of the pharmaceutical industry have become global issues. The effectiveness and reliability of anticancer drugs are determined by a thorough evaluation of their active ingredient content.[22] Due to the significant risk to human health, the detection and delivery methods of such drugs, particularly the synthetic ones, are of enormous interest and concern in the developed world.[23,24] Chlormethine (2-chloro-*N*(2-chloroethyl)-*N*-methylethan-1-amine, CHL) is a well-known nitrogen mustard anticancer drug first synthesized in 1935. It functions by binding to DNA, creating cross-links between DNA strands and thereby inhibiting cell replication. This drug has been extensively used in the treatment of cancers, such as prostate cancer, myelocytic leukemia, and polycythemia vera. However, excessive use of CHL can lead to severe health issues, including bone marrow damage, skin alterations, and even blindness.[25−27] Therefore, developing sensors and drug carriers for accurate detection, quantification, and delivery of CHL could help optimize dosage and reduce its toxicity. Numerous theoretical studies have explored the interaction mechanisms between CHL and fullerene-like structures beyond graphene. For example, Hossain et al. predicted that CHL exhibits more stable adsorption with Ni-decorated boron nitride nanocages in both water and gas phases compared to Fe, Co, Cu, and Zn-decorated nanocages.[27] Another 0D fullerene-like material studied for its interaction with CHL is the $B_{24}O_{24}$ nanocluster, as reported by Gholami and Solimannejad.[28] The adsorption energies of CHL on the $B_{24}O_{24}$ nanocage for the most stable complexes range from −1.47 to −1.36 eV in both the gas phase and aqueous media. Although experimental methods like high-performance liquid chromatography and capillary electrophoresis are used for biosensors and drug delivery systems, their widespread application is limited due to high costs and complex techniques.[29,30] DFT has proven useful in overcoming these experimental limitations by modeling and designing nanomaterials. It offers reliable results at lower costs, is less time-consuming, and presents fewer risks.

Consequently, given its notable properties, the C_{36} fullerene has been selected as the channel material to achieve a high-performance CHL nano sensor and carrier in this study. We employ first-principles DFT to study the CHL adsorption on pristine and metal−metalloid (MM)-modified C_{36}. The choice of metals (Al, Fe) and metalloid (B) for decorating C_{36} fullerenes is driven by their potential to strengthen binding interactions, alter electronic properties, ensure biocompatibility, enhance structural stability, and boost therapeutic effectiveness.[31] Boron (B) has been widely studied due to its ability to enhance binding interactions with fullerene structures, as demonstrated in prior research, making it a promising candidate for modifying electronic properties while maintaining biocompatibility and structural stability.[32−34] Aluminum (Al), on the other hand, is known for its lightweight, cost-effectiveness, and ability to create stronger interactions with fullerene surfaces, which can contribute to the overall stability and therapeutic effectiveness of the functionalized structure.[34] Iron (Fe) has been chosen for its magnetic properties, potential for enhancing electron transfer, and biological relevance, particularly in drug delivery applications.[35] By selection of these elements, our research focuses on identifying the adsorption sites and binding energies of CHL on C_{36} fullerenes with surface modifications. We methodically investigate both the electronic and geometric aspects of these interactions to provide comprehensive insights into the binding mechanism and charge transfer involved in the adsorption process. The calculations demonstrated that decorating the surface of the C_{36} fullerene with MM elements improved its conductivity and enhanced charge transfer, leading to a better CHL adsorption performance. Additionally, the thermal and dynamic stabilities of the modified system were assessed, along with various factors influencing the practical effectiveness of the sensor and carrier material. The expected results are likely to reveal how MM modifications affect the adsorption behavior of organic molecules on surfaces. These findings offer considerable potential for advancements in the sensor technology, drug delivery systems, and chemical catalysis.

2. COMPUTATIONAL DETAILS

To perform the structural optimization of CHL and fullerenes, electronic calculations were conducted using the Gaussian 09 package. The DFT/B3LYP method was applied with the 6-31G(d,p) basis set, incorporating Grimme's D3 dispersion correction. The adsorption energy, E_{ad} is defined as

$$E_{ad} = E_{fullerens/CHL} - (E_{fullerens} + E_{CHL}) \quad (1)$$

Here, $E_{fullerenes}$ corresponds to the energy of the optimized fullerenes, and E_{CHL} and $E_{fullerens/CHL}$ are the energies of the isolated CHL and the optimized fullerenes with the adsorbed CHL, respectively. The highest occupied molecular orbital (HOMO)−lowest occupied molecular orbital (LUMO) energy gap (EG) E_G defined by the difference between the LUMO and HOMO called the HOMO−LUMO energy gap (E_G) and is expressed as

$$E_G = E_{LUMO} - E_{HOMO} \quad (2)$$

Lastly, ab initio molecular dynamics (AIMD) simulations were carried out to investigate the impact of temperature on the interaction of the most stable formed complex.[36,37] AIMD simulations were conducted using the Atom-Centered Density Matrix Propagation (ADMP) method at the B3LYP-D3/6-31G(d,p) level of theory to optimize computational resources. At room temperature (T = 300 K), minimum points in the potential energy surface (PES) were examined and an AIMD simulation ran for 200 fs. According to Gaussian 09 convergence standards, forces, root-mean-square (RMS) force, maximum displacement (predicted displacement for the next step), and RMS displacement should ideally approach zero, meaning that each parameter must fall below its specified threshold. However, an exception exists for large-molecule optimizations, which is especially relevant to organometallic complex design. Specifically, if forces reduce to levels 2 orders of magnitude below the threshold (1/100th of the cutoff), the geometry is considered converged, even if the displacement slightly exceeds its threshold.[38] This criterion is particularly useful in optimizing organometallic geometries as it addresses cases where optimization could continue without energy changes due to a flat PES around the minimum. Once these

https://doi.org/10.1021/acsomega.4c08490
ACS Omega 2024, 9, 49786−49803

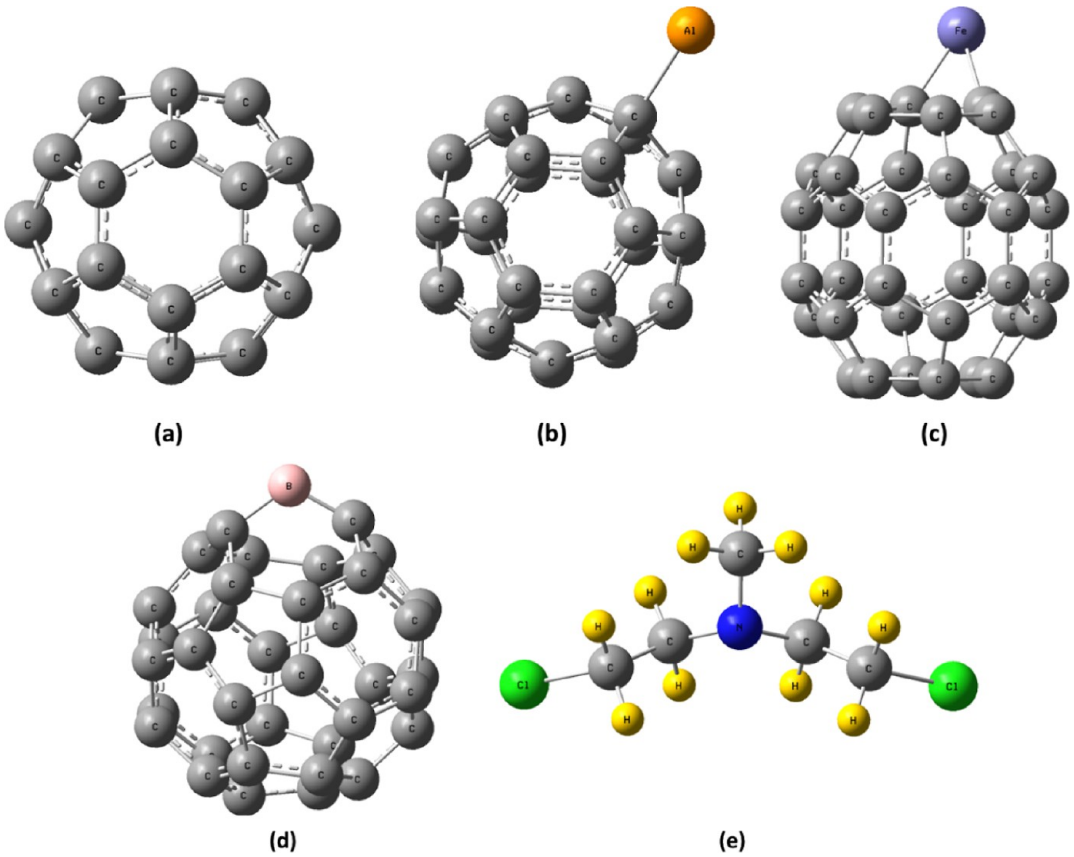

Figure 1. Optimized structure of (a) C_{36}, (b) Al−C_{36}, (c) Fe−C_{36}, and (d) B−C_{36} fullerene and (e) CHL.

conditions are met, the geometry is treated as converged, enabling further calculations of that structure.

3. RESULTS AND DISCUSSION

3.1. Geometry Optimization of the C_{36}, Al−C_{36}, Fe−C_{36}, and B−C_{36} Fullerene and CHL. This section provides a detailed analysis of the interaction between the chosen anticancer drug CHL and both pristine and MM-modified C_{36} fullerene. Initially, all selected molecular structures—including C_{36}, Al−C_{36}, Fe−C_{36}, B−C_{36} fullerene, and the CHL drug molecule—were optimized using DFT-D3/B3LYP with the 6-31G(d,p) basis set. The resulting optimized geometries are illustrated in Figure 1. We began by optimizing the pristine C_{36} fullerene, which belongs to the D_{6h} point group and features both hexagonal and pentagonal rings. The bond lengths observed in the C_{36} structure are 1.365 Å for C═C bonds and 1.463 Å for C═C bonds. The calculated energy gap (E_G) is 1.092 eV, with HOMO and LUMO energies of −5.184 and −4.092 eV, respectively (refer to Table 1). The calculated bond lengths and EG show a good correlation with the previously reported literature.[18−21] To enhance the adsorption mechanism and stability, the pristine C_{36} fullerene was further modified by incorporating MM elements such as Al, Fe, and B. Considering the various feasible adsorption sites on the C_{36} fullerene, we carried out geometry optimizations and calculated the total energy for all MM-C_{36} models. The binding energies of the MM elements on C_{36} were determined by using the following binding energy equation.

$$\Delta E_B = E_{C36+MM} - (E_{C36} + E_{MM}) \quad (3)$$

Table 1. Calculated Values of HOMO−LUMO Gap (E_G), Cohesive Energy (E_C), Binding Energy (ΔE_B), and Binding Distances (d) of the MMs for the Fullerenes

system	E_g (eV)	E_C (eV/atom)	ΔE_B (kJ/mol)	d (nm)
C_{36}	1.093	−8.252		
Al−C36	1.967^{α}	−8.085	−203.48	0.209
	1.973^{β}			
Fe−C36	1.094	−8.027	−277.86	0.189
B−C36	1.923^{α}	−8.132	−369.42	0.141
	1.973^{β}			

In this study, E_{C36+MM} and E_{MM} represent the energies of the modified C_{36} fullerene and the individual MM atom, respectively. Notably, the MM showed a strong preference for binding above the C site, where it achieved the highest binding energy. The corresponding binding energies and distances are detailed in Table 1.

In this study, E_{C36+MM} and E_{MM} represent the energies of the modified C_{36} fullerene and the individual MM atom, respectively. Notably, the MM showed a strong preference for binding above the C site, where it achieved the highest binding energy. The corresponding binding energies and distances are detailed in Table 1.

The B atom demonstrates the strongest binding to the surface of C_{36}, followed by Fe and Al, with binding energies of −369.42, −277.86, and −203.48 kJ/mol, respectively. As shown in Figure 1, the relaxed geometries of the MM-modified C_{36} structures reveal that the B, Fe, and Al atoms protrude above the C atom of the C_{36} fullerene, with the shortest distances being 0.141, 0.189, and 0.209 nm, respectively (for

https://doi.org/10.1021/acsomega.4c08490
ACS Omega 2024, 9, 49786−49803

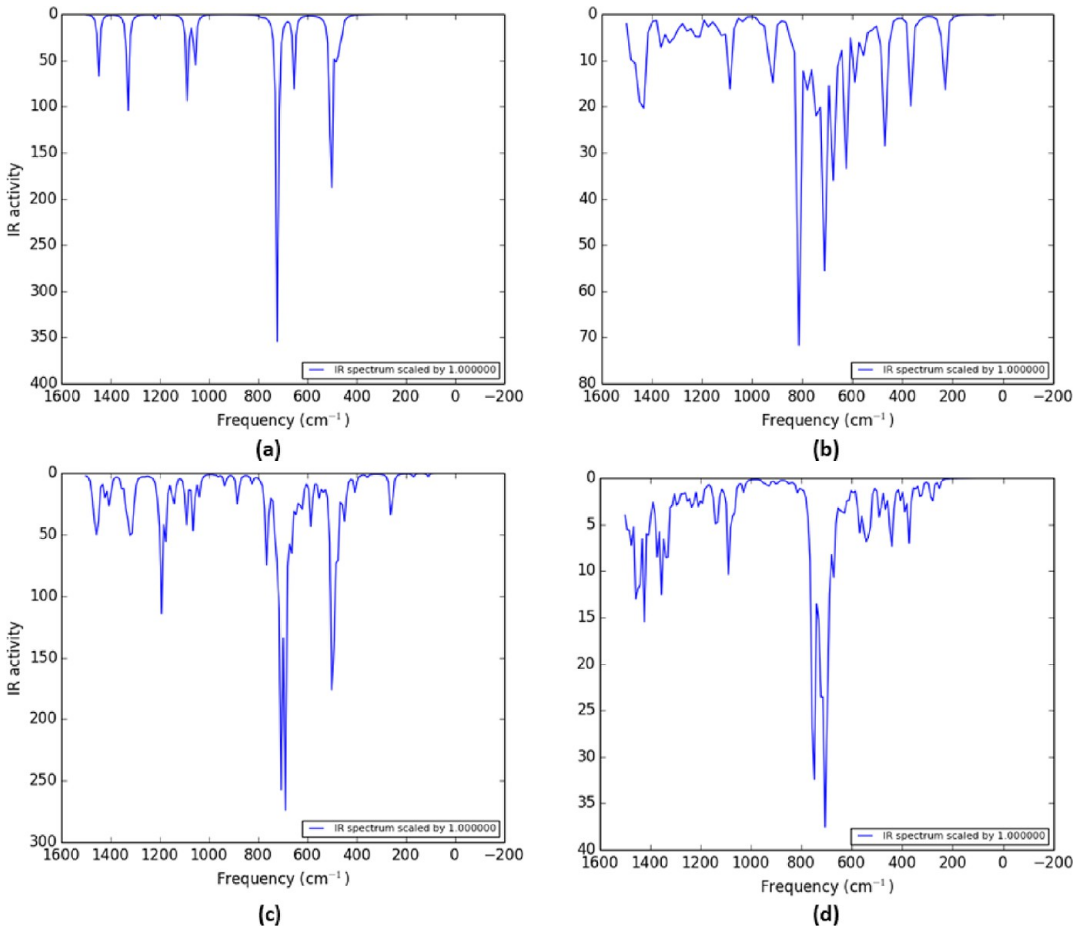

Figure 2. IR of (a) C_{36}, (b) Al−C_{36}, (c) Fe−C_{36}, and (d) B−C_{36} fullerene.

the optimized coordinates, see Supporting Information Section S9). The significant binding energy and minimal binding distance indicate that the MMs establish a covalent bond with the C atoms on the surface of C_{36} fullerene. This strong bonding is crucial for ensuring the stability of the system.

We also computed the cohesive energies (E_c) for both the pristine and modified fullerenes, as shown in Table 1. Their stability is confirmed by the high magnitudes and negative values of these cohesive energies. To further validate stability, we examined the infrared (IR) spectrum frequencies by analyzing the vibrational modes. We found that all the vibrational modes of the selected fullerenes exhibit real frequencies, ranging between 200 and 1600 cm^{-1} (Figure 2). Figure 3 illustrates the electron density distributions for the HOMO and LUMO orbitals of the selected fullerenes. The frontier molecular orbitals (FMOs), which include the HOMO and the LUMO, are crucial for investigating the electronic properties of smaller fullerenes.[39] The HOMO, located on the donor moiety, acts like a valence band, whereas the LUMO, positioned on the acceptor moiety, functions similarly to a conduction band. The band gaps (E_G) are defined as the energy difference between the HOMO and LUMO levels (see Table 1). There is an inverse correlation between the molecular band gap (E_G) and reactivity. Molecules with low E_G values generally show decreased stability and softer characteristics, but they also exhibit enhanced charge transport capabilities. In the HOMO and LUMO structures, green and red colors represent the negative and positive phases, respectively.[40] Notably, Figure 3 demonstrates a uniform distribution pattern of the HOMO and LUMO orbitals across the MM-modified fullerenes. In our study, we observed alpha (α) and beta (β) contributions to the HOMO−LUMO gap in B- and Al-decorated C_{36} fullerenes. The addition of B or Al induces electron transfer, either donating or withdrawing electrons from the C_{36} cage. This electron transfer leads to a splitting of the alpha and beta orbitals, creating distinct HOMO and LUMO levels for each spin state. For all four fullerenes, the LUMO is primarily located near the outer surface of the spherical structure. Conversely, the HOMO for each fullerene exhibits a higher electron density toward the center of the sphere and a lower density on the outer surface. Moreover, we observed a notable localization of HOMO and LUMO electron densities at the edges of MM-decorated fullerenes, unlike in the pristine C_{36}. Finally, after confirming the ground-state properties of the various fullerenes, we proceeded to optimize the CHL drug molecule.[27,28,41,42]

We performed electrostatic potential (ESP) mapping to identify the optimal sites for potential interactions. Figure 4 displays the charge distribution for both the systems and the CHL molecule. In the ESP mapping, red areas indicate regions of high electron density and attractive or negative potential, while blue areas denote regions of electron deficiency or positive potential, with neutral regions in between. For pristine C_{36}, blue regions were observed in the hollow portions. However, in the MM-decorated C_{36} cases, these blue regions shift toward the MM atoms. In the cases of B and Fe decoration, we observed a pronounced positive potential region at the B and Fe sites, compared to the Al case.

https://doi.org/10.1021/acsomega.4c08490
ACS Omega 2024, 9, 49786−49803

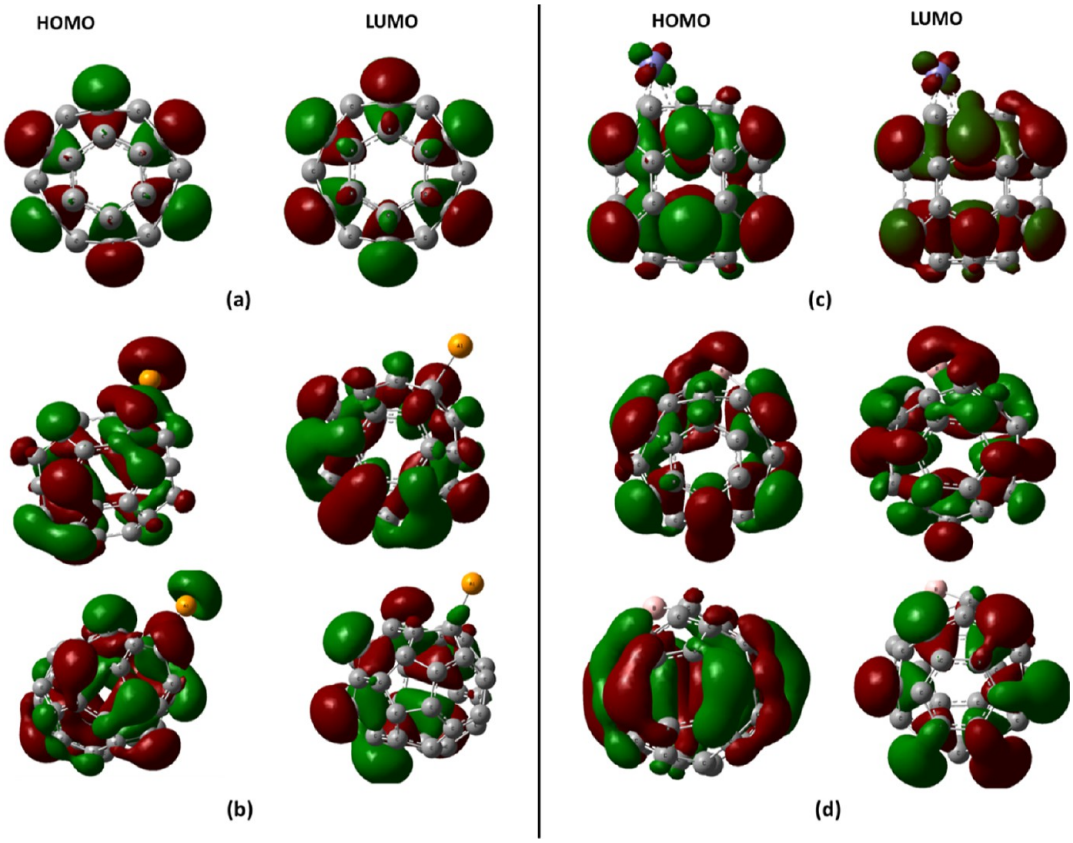

Figure 3. LUMO and HOMO electron contribution of (a) C_{36}, (b) Al−C_{36} (α and β), (c) Fe−C_{36}, and (d) B−C_{36} (α and β) fullerene.

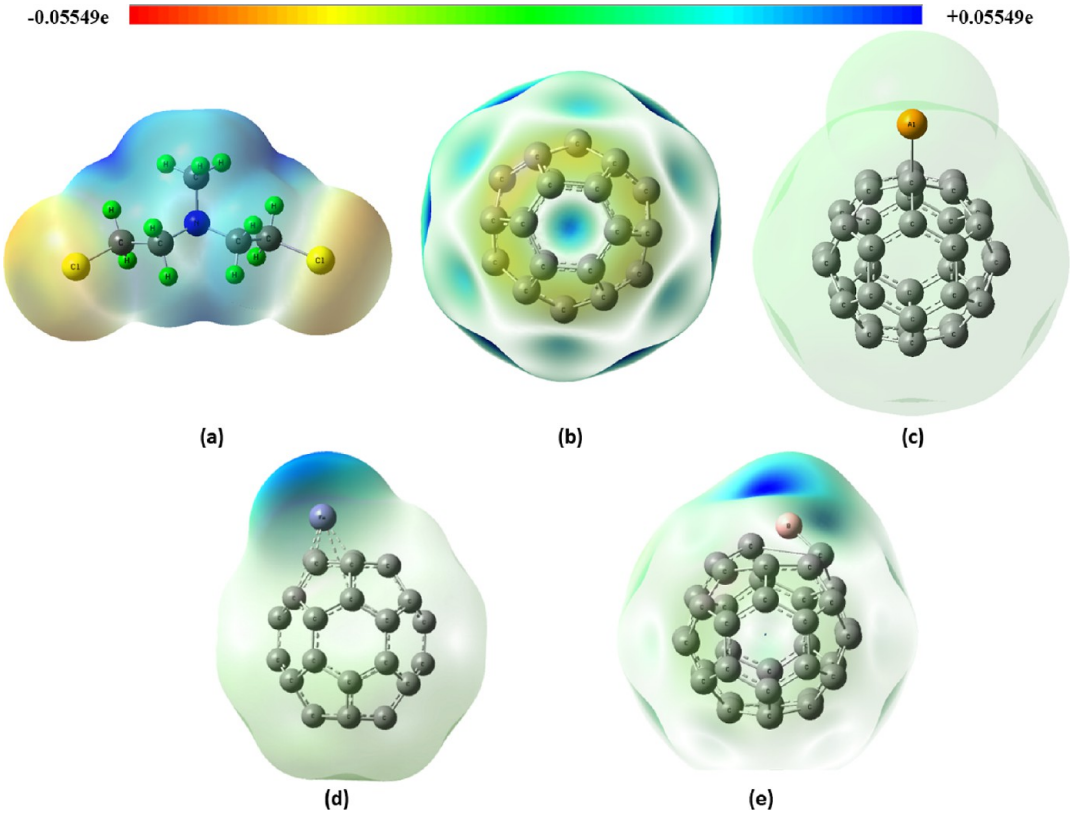

Figure 4. ESP of (a) CHL, (b) C_{36}, (c) Al−C_{36}, (d) Fe−C_{36}, and (e) B−C_{36} fullerene (EPS) from −0.05549e to 0.05549e.

https://doi.org/10.1021/acsomega.4c08490
ACS Omega 2024, 9, 49786−49803

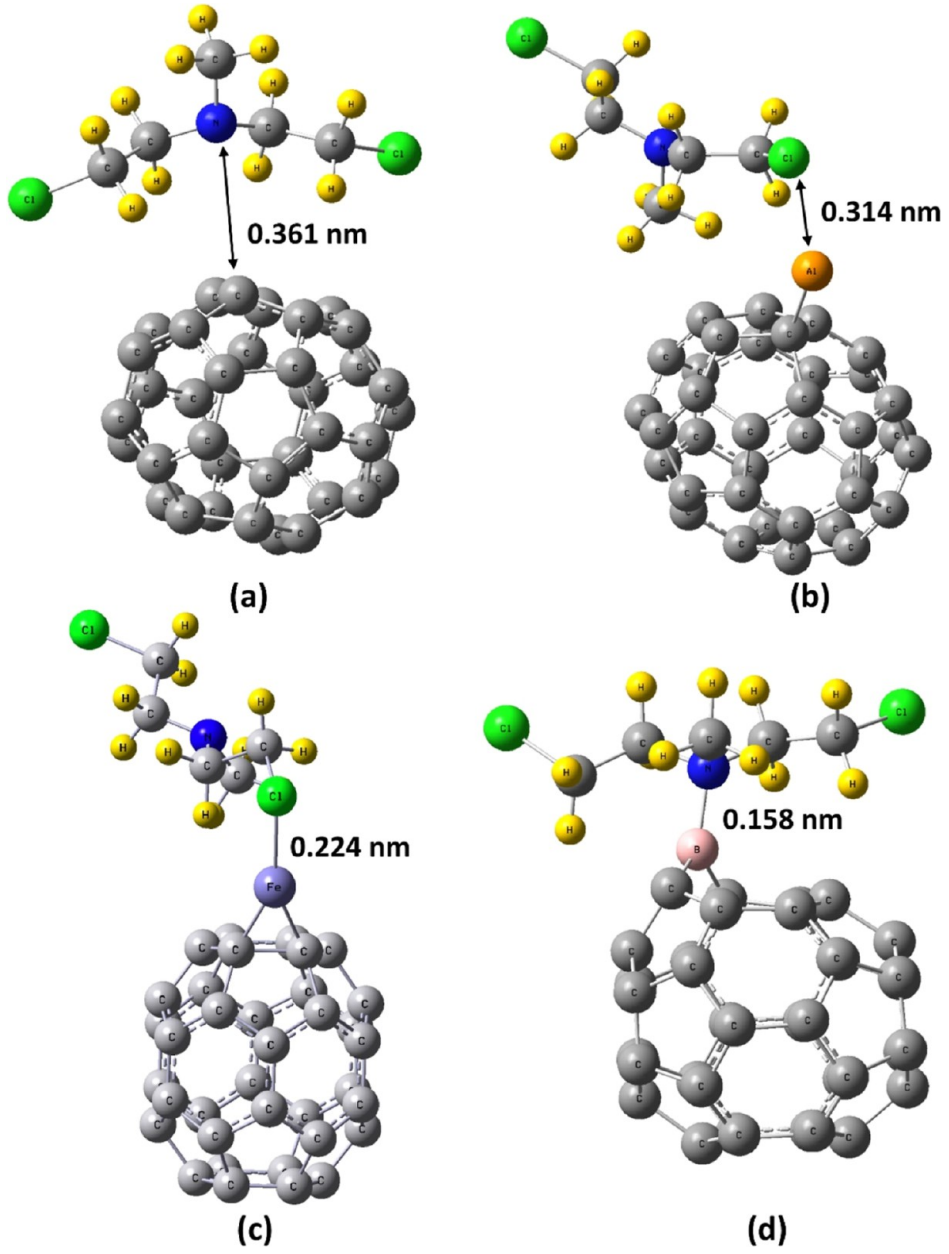

Figure 5. Minimum energetic geometry of CHL adsorbed over (a) C_{36}, (b) Al−C_{36}, (c) Fe−C_{36}, and (d) B−C_{36} fullerene, respectively.

Table 2. Calculated Value of Adsorption Energy (E_{ad}), LUMO Energy (E_{LUMO}), Fermi Level (E_F), HOMO Energy (E_{HOMO}), HOMO−LUMO Gap (E_G), Relative Change in E_F (ΔE_{FR}), Relative Change in E_G (ΔE_{GR}), and Adsorption Distance (d) of CHL Adsorbed over C_{36}, Al−C_{36}, Fe−C_{36}, and B−C_{36} Fullerene, Respectively

complex	E_{ad} (kJ/mol)	E_{LUMO} (eV)	E_f (eV)	E_{HOMO} (eV)	E_G (eV)	E_{FR} (%)	E_{GR} (%)	d (nm)
C_{36}/CHL	−39.07	−4.092	−4.630	−5.184	1.092	0.795	−0.12441	0.361
Al−C_{36}/CHL	−41.87	-3.358^{α}	-4.320^{α}	-5.292^{α}	1.933^{α}	0.64586^{α}	-1.742^{α}	0.315
		-3.471^{β}	-4.450^{β}	-5.425^{β}	1.954^{β}	0.758^{β}	-0.993^{β}	
Fe−C_{36}/CHL	−141.83	−3.377	−3.928	−4.477	1.099	−4.5432	0.44743	0.224
B−C_{36}/CHL	−179.26	-2.875^{α}	-3.750^{α}	-4.624^{α}	1.749^{α}	-15.415^{α}	-9.039^{α}	0.158
		-3.108^{β}	-3.940^{β}	-4.773^{β}	1.665^{β}	-13.245^{β}	-15.632^{β}	

Additionally, the chlorine atoms in the CHL drug molecule exhibit strongly negative electron regions. There are no significant changes when the CHL molecule and the corresponding fullerenes are reoptimized in the aqueous phase.

3.2. Adsorption Properties of the CHL Drug Molecule over Pristine and MM-Modified C_{36} Fullerene. We have explored the most stable arrangement of the CHL drug molecule in interaction with both pristine and MM-modified fullerenes, aiming to confirm its binding affinity for these fullerenes (Figure 5). It has been noted that the CHL drug molecule interacts with fullerenes while maintaining its structural integrity. The hexagonal and pentagonal rings of

https://doi.org/10.1021/acsomega.4c08490
ACS Omega 2024, 9, 49786−49803

the pristine fullerenes, along with the MM atom sites on the MM-decorated C_{36} fullerene, serve as key platforms for the interaction mechanism with the CHL (refer to the ESP mapping). Various possible adsorption sites for the drug molecule on fullerenes have been examined to identify the lowest energy conformer. For the pristine C_{36} fullerene, CHL is adsorbed with an energy of −39.07 kJ/mol across the hexagonal ring of C_{36}. The optimized separation between the CHL drug molecule and the C_{36} fullerene is 0.361 nm, indicating a physisorption interaction. ESP studies reveal that CHL favors adsorption onto the B−C_{36} fullerene through the N-atom rather than the H-atom due to the presence of additional electrons. The adsorption energy of the CHL drug molecule on B−C_{36} is −179.26 kJ/mol, with the distance between the nitrogen (N) atom of CHL and the boron (B) atom of B−C_{36} being approximately 0.158 nm (see Table 2). Chemisorption is the process responsible for the strong attachment of the CHL drug molecule to the B−C_{36} fullerene.[17] Additionally, CHL is physically adsorbed onto the hexagonal sites of Al−C_{36} fullerene with an adsorption energy of −41.87 kJ/mol. The minimum distance between the drug molecule and Al−C_{36} fullerene is 0.314 nm. Finally, the CHL drug molecule demonstrates strong adsorption onto the Fe−C_{36} fullerene with an adsorption energy of −141.83 kJ/mol. The distance between the chlorine (Cl) atom of CHL and the iron (Fe) atom of Fe−C_{36} is approximately 0.224 nm. Although this distance might initially appear to fall within the range typically associated with physisorption, further analysis indicates that this interaction is likely chemisorption in nature. Supporting this, the literature reports Fe−Cl bond lengths of approximately 0.231 nm in crystalline $FeCl_3$, which is closely aligned with our observed bond length. This similarity strongly suggests the formation of a chemical bond between the Fe and Cl atoms.[43] The calculated adsorption energy of −141.83 kJ/mol further corroborates the classification of this interaction as chemisorption as such energy values are generally consistent with chemical bonding rather than weak physisorption interactions.[44] The adsorption energies provide insight into the nature and preference of the drug molecule for the fullerenes.

To examine the effect of basis set superposition error (BSSE) correction on the interaction between the CHL drug molecule and MM-modified C_{36} fullerene, we calculated and compared the total energy with and without BSSE correction (refer to Table S1 in Section S1 of the Supporting Information) using the B3LYP/6-31G(d,p) method with GD3.[45] Results from Section S1 of the Supporting Information show only a negligible difference in total energy values, indicating consistency with those obtained using BSSE correction.

To gain deeper insights, we also calculated and compared the adsorption energies of CHL on MM-modified C_{36} fullerenes using both the B3LYP/6-311G + + (d, p) and ωB97XD/6-311G + + (d, p) methods (detailed in Section S2 of the Supporting Information). Our results indicate that CHL exhibits strong chemisorption interactions with Fe−C_{36} and B−C_{36} fullerenes, while the other fullerenes primarily show physisorption. Importantly, the findings are consistent across both computational approaches.[46]

To ensure local minima and the lowest energy configurations, it is crucial to validate vibrational calculations. The presence of real frequencies and minimum energy configurations confirms the local minima of the complexes. All MM-modified C_{36} fullerene systems exhibit real frequencies, indicating that they are dynamically stable.[47] In our study, we computed the IR spectra for all complexes, which are presented in Figure S2 of Section S5 in the Supporting Information. The IR spectra were analyzed within the wavenumber range of 0 to 1600 cm^{-1}, as discussed in Section S5 of the Supporting Information.

We additionally calculated the adsorption energy with zero-point energy corrections and performed ESPmapping for the CHL drug after its interaction with the fullerenes (refer to Supporting Information Sections S3 and S4, respectively). To further understand the quantum mechanical foundation of this preference, we carried out natural bond orbital (NBO) and Mulliken charge analyses.

3.3. NBO Charge Analysis. Understanding the electronic charge transfer is crucial for comprehending the interaction between an adsorbate and an adsorbent. The NBO analysis, as shown in Table 3, offers insight into the charge transfer that occurs between selected fullerenes and drug molecules during adsorption, particularly in their optimized geometrical configurations.[16] We also analyzed the Mulliken population to determine the direction of spontaneous charge flow in the interactions between the fullerenes and the drug molecule.[48] Upon adsorption onto C_{36}, B−C_{36}, Al−C_{36}, and Fe−C_{36}, the net Mulliken charge of the CHL drug molecule was found to be −0.029e, +0.298e, +0.01e, and +0.144e, respectively. As the isolated drug molecule has no net Mulliken charge, the positive Mulliken charge values observed for the drug molecule in MM-decorated fullerenes indicate that the charge is transferred from the CHL to the fullerene.[48−50] The charge distribution of CHL adsorbed onto the selected fullerenes is illustrated in Figure 6. Similarly, the NBO calculation was employed to elucidate the second-order perturbation stabilization energy, $E^{(2)}$, for the donor−acceptor (bond−antibond) interactions between the selected fullerenes and LEU, as predicted by the second-order Fock matrix. The equation for the second-order perturbation stabilization energy, $E^{(2)}$, describing the delocalization from the donor (i) to the acceptor (j), is given as follows[16]

$$E^{(2)} = \Delta E_y = q_i \frac{F^{(2)}(ij)}{\varepsilon_i - \varepsilon_j} \tag{4}$$

It is well established that the second-order perturbation stabilization energy is directly proportional to the intensity of the NBO interactions. A stronger interaction between the donor and acceptor leads to a higher stabilization energy, thereby enhancing the stability of fullerene/drug molecule complexes.[51] In this case, Table 3 presents only the highest values of $E^{(2)}$. The data indicate that in the B−C_{36}/CHL complex, the (N40) atom of CHL serves as the donor, while the (B37) atom of the B−C_{36} fullerene acts as the acceptor.

Table 3. NBO Second-Order Perturbation Energy (E^2, kcal/mol) Corresponds to the Charge Transfer between the CHL and C_{36}, Al−C_{36}, Fe−C_{36}, and B−C_{36} Fullerene, Respectively

system	donor	acceptor	$E^{(2)}$ (kcal/mol)
C_{36}/CHL	LP(Cl37)	LP*(C13)	0.76
Al−C_{36}/CHL	LP(Cl38)	LP*(Al37)	4.67
Fe−C_{36}/CHL	LP(Cl38)	LP*(Fe37)	39.41
B−C_{36}/CHL	LP(N40)	LP*(B37)	101.87

https://doi.org/10.1021/acsomega.4c08490
ACS Omega 2024, 9, 49786−49803

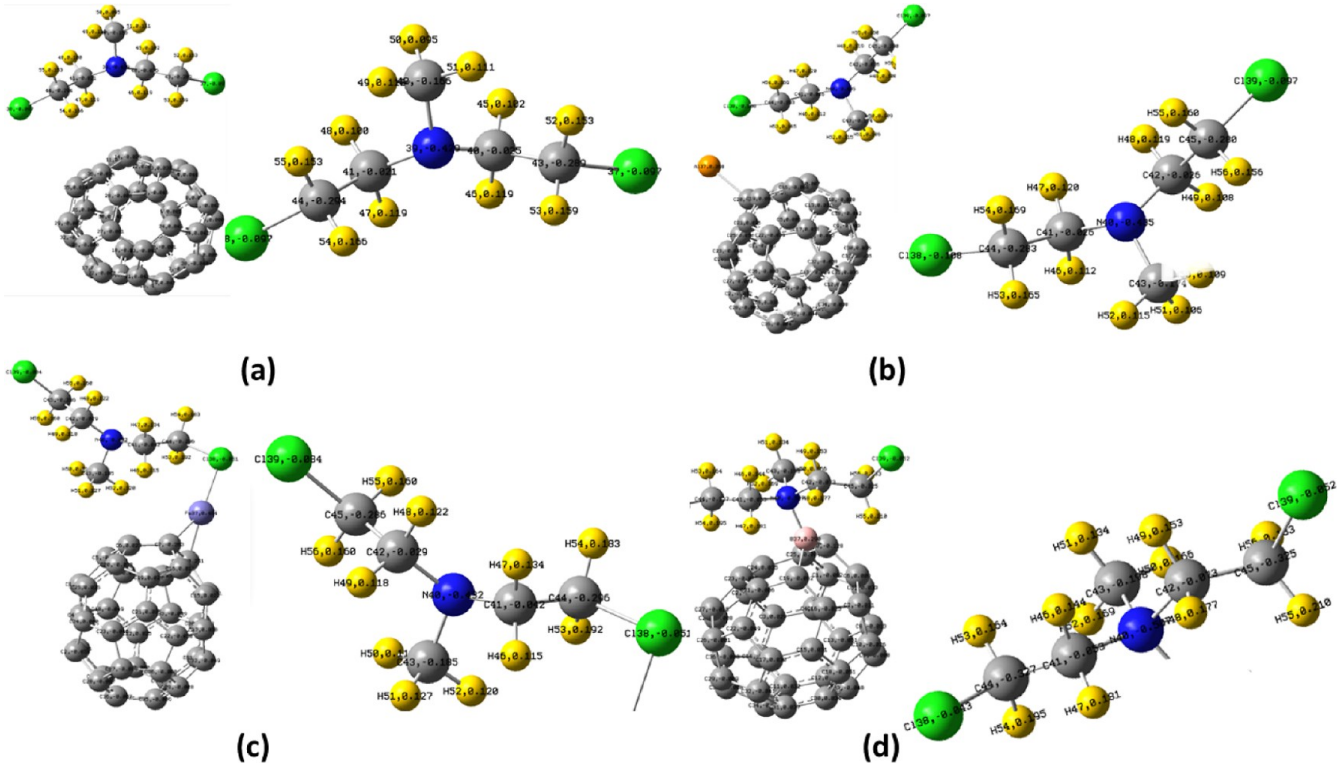

Figure 6. Mulliken charge population analysis of CHL adsorbed over (a) C_{36}, (b) Al−C_{36}, (c) Fe−C_{36}, and (d) B−C_{36} Fullerene, respectively.

Table 4. QTAIM Parameters of the Selected CHL Adsorbate over C_{36}, Al−C_{36}, Fe−C_{36}, and B−C_{36} Fullerene, at the BCPs[a]

complex	bond	ρ_{BCP}	$\Delta^2\rho_{BCP}$	G_{BCP}	V_{BCP}	H_{BCP}	$\lvert V_{BCP}\rvert/G_{BCP}$
C_{36}/CHL	Cl37−C13	0.0047063566	0.0127671258	0.0024278355	−0.0016638895	0.0007639459	0.685
Al−C_{36}/CHL	N40−B37	0.1543110336	0.0143162982	0.1406670893	−0.2777551041	0.1370880148	1.97
Fe−C_{36}/CHL	Cl38−Al37	0.0090559690	0.0075944777	0.0012059784	−0.0025133374	−0.0003073590	2.085
B−C_{36}/CHL	Cl38−Fe37	0.0773195295	0.1934252424	0.0662556697	−0.0841550288	−0.0178993591	1.27

[a]Electron density ($\rho(r)$), Laplacian of electron density ($\nabla^2\rho(r)$), the kinetic energy density ($G(r)$), potential energy density ($V(r)$), total electron energy density ($H(r)$), and the ratio $|V_{BCP}|/G_{BCP}$.

Similarly, in the Fe−C_{36}/CHL complex, the (Cl38) atom of CHL functions as the donor, and the (Fe37) atom of the Fe−C_{36} fullerene serves as the acceptor. The ESP results are consistent in both cases. The higher values of $E^{(2)}$, which are 101.87 kcal/mol for the B−C_{36}/CHL complex and 39.41 kcal/mol for the Fe−C_{36}/CHL complex, indicate a stronger interaction between the fullerene and the CHL drug molecule. The adsorption of CHL on B−C_{36} and Fe−C_{36} fullerenes shows a significant charge transfer and high adsorption energy, suggesting that chemisorption is the predominant adsorption mechanism. In contrast, the minimal $E^{(2)}$ values for the C_{36}/CHL and Al−C_{36}/CHL complexes are 0.76 and 4.67 kcal/mol, respectively. The physisorption nature of the adsorption between CHL and C_{36}, as well as Al−C_{36}, is evidenced by the lower $E^{(2)}$ values observed in comparison to those of the B−C_{36}/CHL and Fe−C_{36}/CHL complexes. In simple terms, the primary interaction occurs between the lone pairs of the CHL drug molecule, which act as donors, and the LP* of the fullerenes, which function as acceptors.

3.4. QTAIM Analyses. To further investigate the interactions between the CHL drug molecule and both pristine and MM-decorated fullerene structures, we utilized a Topology Analysis approach based on Bader's quantum theory of atoms in molecules, using the MULTIWFN software tool.[52] Topology parameters, derived from the electron density at critical bond sites (BCPs) through QTAIM analysis, is used to characterize intermolecular interactions in this system, as detailed in the corresponding Table 4. In QTAIM analysis, we focus on key parameters such as electron density ($\rho(r)$) and the Laplacian of the electron density ($\nabla^2\rho(r)$), which are conventionally used to distinguish between different bonding interactions. Additionally, we incorporate the total energy density ($H(r)$) and the ratio of the potential energy density $|V(r)|$ to the kinetic energy density $G(r)$ as these provide further insights into the strength and character of the interactions. It is important to recognize that these measurements highlight unique characteristics specific to various types of interactions. By examining the conditions where $\nabla^2\rho(r) > 0$, $H(r) > 0$, and $|V(r)|/(G(r)) < 1$, we can differentiate between weak and medium-strength hydrogen bonds as well as van der Waals (vdW) interactions. For strong hydrogen bonds, which represent an intermediate interaction type, the indicators are $\nabla^2\rho(r) > 0$, $H(r) < 0$, and $1 < |V(r)|/G(r) < 2$. In contrast, covalent bonding is characterized by $\nabla^2\rho(r) < 0$, $H(r) < 0$, and $|V(r)|/G(r) > 2$.[53,54]

Table 4 displays the QTAIM parameters calculated for both pristine and MM-decorated fullerenes with CHL. Figure 7 illustrates the molecular topographical map of the CHL drug

https://doi.org/10.1021/acsomega.4c08490
ACS Omega 2024, 9, 49786−49803

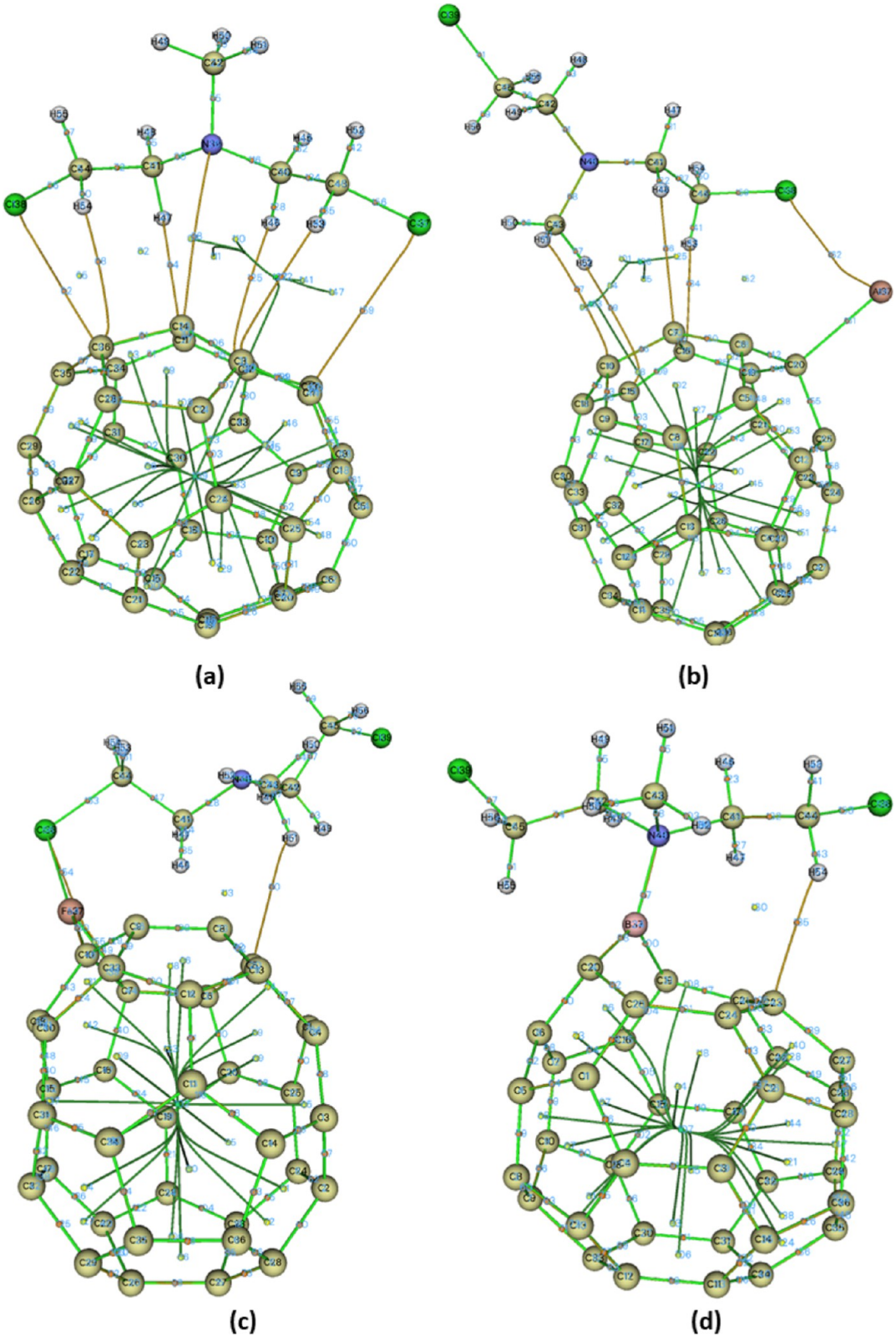

Figure 7. Computed molecular topographical map of (a) C_{36}/CHL, (b) Al−C_{36}/CHL, (c) Fe−C_{36}/CHL, and (d) B−C_{36}/CHL with all critical points. Atomic and bond critical points are presented by atom labels and orange spheres, respectively. The cage and ring critical points due to green and yellow circles. The lines are bond paths.

molecule on fullerenes, highlighting key locations. The computational results presented in Table 4 reveal various interactions between the drug molecule and the system. Notably, the interactions between the B−C_{36}/CHL and Fe−C_{36}/CHL systems are classified as strong hydrogen bonds with a semicovalent character. This term refers to an interaction that exhibits features of both covalent and noncovalent bonding, where the electron density at the bond critical points

https://doi.org/10.1021/acsomega.4c08490
ACS Omega 2024, 9, 49786−49803

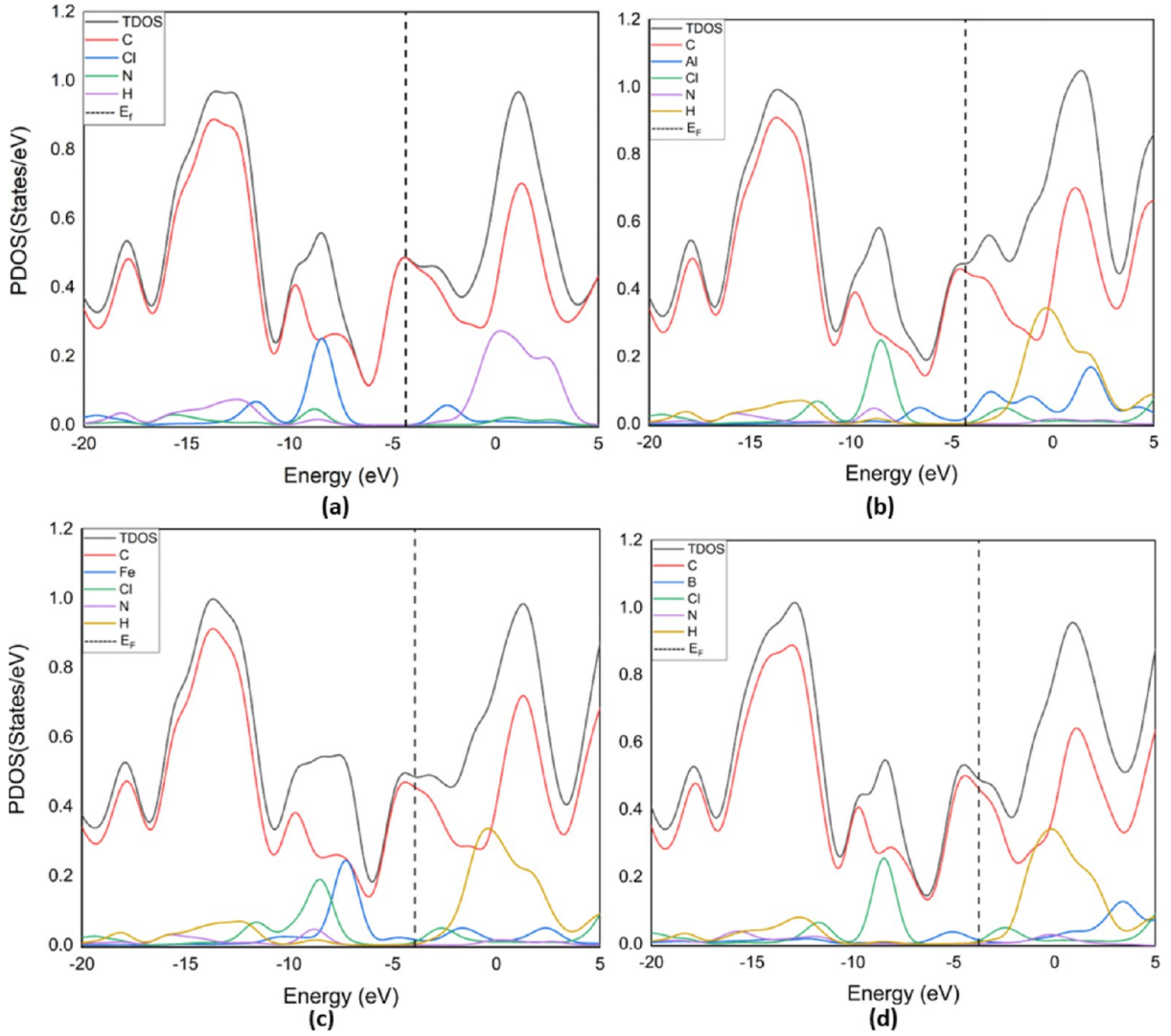

Figure 8. TDOS and PDOS for of (a) C_{36}/CHL, (b) Al−C_{36}/CHL, (c) Fe−C_{36}/CHL, and (d) B−C_{36}/CHL complexes.

indicates a significant degree of electron sharing, yet the bond remains somewhat polar. Specifically, these interactions are characterized by $\nabla^2\rho(r) > 0$, $H(r) < 0$, and $1 < |V(r)|/G(r) < 2$, which suggests that the bonds possess an intermediate nature between covalent and electrostatic interactions. Conversely, the other interactions observed for both systems predominantly reflect weak vdW forces, as indicated by QTAIM parameters consistent with noncovalent interactions, dominated by electrostatic contributions.[55,56]

3.5. Density of States Analysis. In addition to the previously analyzed parameters, the electronic interactions between CHL and both pristine and MM-modified C_{36} fullerenes can be further investigated through density of states (DOS) plots following the adsorption of the drug molecule. Figure 8 presents the calculated and plotted total DOS (TDOS) and partial DOS (PDOS). PDOS is used to determine the contributions of molecular orbitals and primarily reflects the composition of the fragment orbitals, while TDOS is crucial for monitoring changes in the band gap. All of the complexes exhibited bonding characteristics, with DOS values ranging between 0 and 1. Table 2 displays the estimated HOMO and LUMO energies as well as the changes in the Fermi level and band gap fluctuations in percent. After the adsorption of CHL onto B−C_{36} fullerene, the HOMO and LUMO energies in the alpha contribution shift from −5.395 eV and −3.471 eV to −4.624 eV and −2.875 eV, respectively, reflecting a 9.039% change in the HOMO−LUMO gap. Additionally, for Fe−C_{36} fullerene, the HOMO and LUMO energy levels are initially −4.662 and −3.567 eV, respectively.

Following interaction with CHL, these levels shift to −3.377 and −4.030 eV, resulting in a 4.5432% change in the Fermi energy level (Table 2). No significant changes in the HOMO−LUMO gap or Fermi level are observed for the other fullerenes after CHL adsorption. Among all of the complexes, the B−C_{36}/CHL and Fe−C_{36}/CHL complexes show the most significant changes in both E_G and E_F, indicating that chemisorption occurs between them. Figure 9 illustrates the localization of the HOMO electron density, highlighting the connection between the nitrogen (N) and chlorine (Cl) atoms of the CHL drug molecule and the nearest B and Fe atoms of B−C_{36} and Fe−C_{36} fullerenes, respectively. This observation confirms the presence of a chemical bond, indicating a strong interaction between CHL and the B−C_{36} and Fe−C_{36} fullerenes. The localization of HOMO and LUMO electron densities for CHL adsorbed onto pristine C_{36} and Al−C_{36}

https://doi.org/10.1021/acsomega.4c08490
ACS Omega 2024, 9, 49786−49803

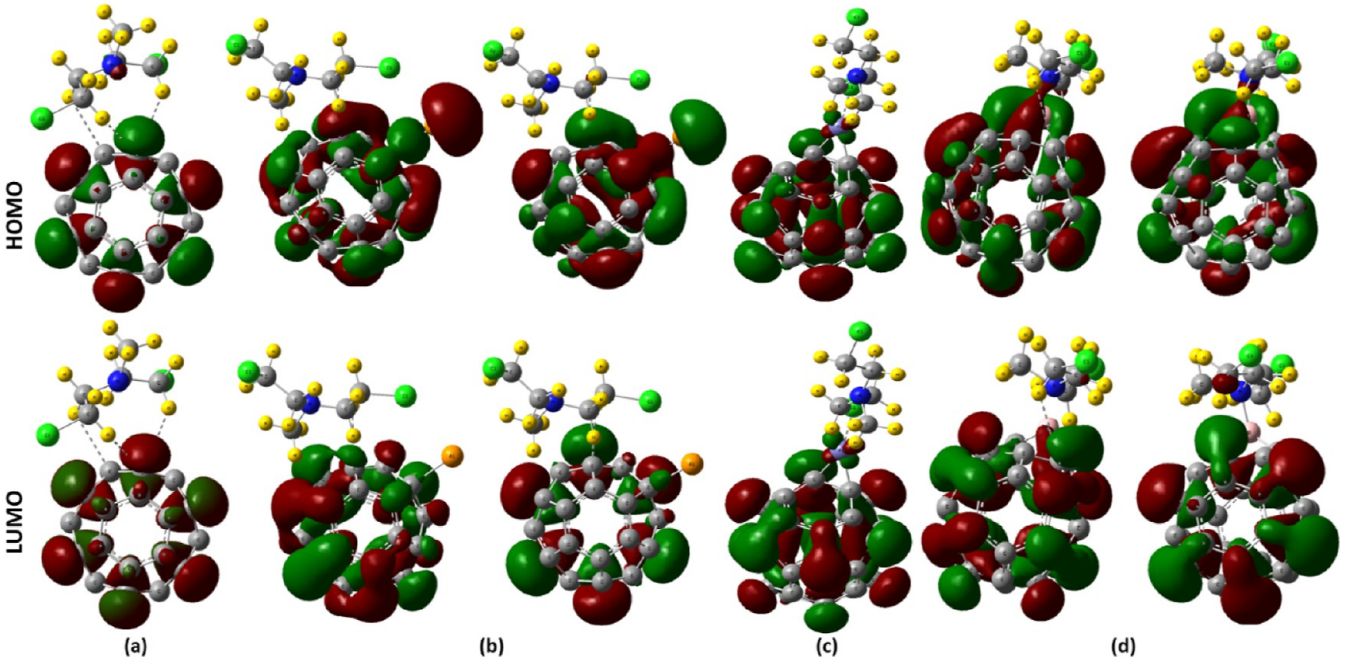

Figure 9. LUMO and HOMO electron density of CHL adsorbed over the (a) C_{36}, (b) Al−C_{36} (α and β), (c) Fe−C_{36}, and (d) B−C_{36} (α and β) fullerene, respectively.

fullerenes demonstrates the optimal adsorption energies between these systems.

3.6. Reduced Density Gradient Analysis. To understand the attraction and repulsion in interactions and to evaluate the nature of weak or strong interactions in CHL/fullerene complexes, Figure 10 presents scatter plots of the reduced density gradient (RDG) versus sign($\lambda 2$)ρ, along with noncovalent interaction (NCI) isosurfaces.[57] Stronger attractive interactions, such as hydrogen bonds and dipole−dipole interactions, are indicated by more negative values of sign($\lambda 2$) with a charge density (ρ) of −0.04. In contrast, strong steric interactions are represented by positive values of sign $\lambda 2$ with a charge density of 0.04. VdW forces are similarly associated with a charge density around ρ = 0.[58] NCI isosurface plots reveal that blue regions represent strong interactions, red regions indicate strong steric effects, and green regions correspond to vdW interactions. As shown in Figure 10c,d, the adsorption of the CHL drug molecule onto B−C_{36} and Fe−C_{36} results in an increase in the number of RDG points (around 0.8 on the y-axis) in areas of strong attractive interactions. VdW forces are present for the C_{36}/CHL and Al−C_{36}/CHL complexes, respectively, near ρ = 0, as shown in Figure 10a,b, supporting the physisorption nature of their adsorption interactions.

The stronger interaction of CHL with B- and Fe-decorated C_{36} fullerenes, in contrast to pristine and Al-decorated C_{36}, can be attributed to several important factors. The incorporation of B and Fe modifies the electronic structure of the fullerene surface, creating more favorable conditions for CHL adsorption. This is largely due to the distinct charge redistribution caused by these elements, which enhances the binding affinity. Additionally, Fe's d-orbital involvement and the electron-deficient nature of B lead to stronger orbital interactions with CHL, improving the binding efficiency. Moreover, the surface reactivity of B- and Fe-decorated C_{36} is higher, as these atoms introduce defects or reactive sites, increasing the chemical activity of the surface and facilitating stronger interactions with CHL. The magnetic properties of Fe further contribute to stabilizing the CHL binding, potentially introducing additional mechanisms for enhanced adsorption. Enhanced electrostatic interactions, such as increased dipole moments or charge transfer, further strengthen the binding between the CHL and the decorated fullerenes.

3.7. Sensing Response. The effectiveness of a chemical sensor, which relies on the energy gap (E_G), can potentially be optimized through a thorough understanding of its experimental sensing properties.[59] To analyze how variations in the electronic properties of fullerenes influence their electrical conductivity or resistivity, the following equation can be employed using the E_G.[60−62]

$$\sigma = AT^{3/2}\exp(-E_G/KT) \tag{5}$$

In this context, σ represents electrical conductivity, A is a constant, K denotes the Boltzmann constant, and T represents the operating temperature. We calculate the sensing response using eq 4, which employs this formula to illustrate the effectiveness of the sensing materials.[63]

$$S = |(\sigma_1/\sigma_2) - 1| = \exp(|\Delta E_G|/KT) - 1 \tag{6}$$

The energy gaps for the complex and the fullerenes are denoted as E^{G2} and E^{G1}, respectively, with ΔE_G defined as ($E^{G2} - E^{G1}$).

The HOMO−LUMO band gap of the B−C_{36} fullerene was significantly altered by adsorption of the CHL drug molecule (Table 2). This adsorption led to a notable shift in the energy gap (E_G) of the fullerene, indicating that B−C_{36} exhibits a high sensitivity to the CHL drug molecule. Our investigation reveals that the B−C_{36} fullerene shows the most favorable sensing response to CHL, with an alpha contribution of approximately 19117.14 at 300 K (Table 5). In contrast, the sensing responses of the other complexes—C_{36}/CHL, Al−C_{36}/CHL, and Fe−C_{36}/CHL—are less impressive due to the minimal

https://doi.org/10.1021/acsomega.4c08490
ACS Omega 2024, 9, 49786−49803

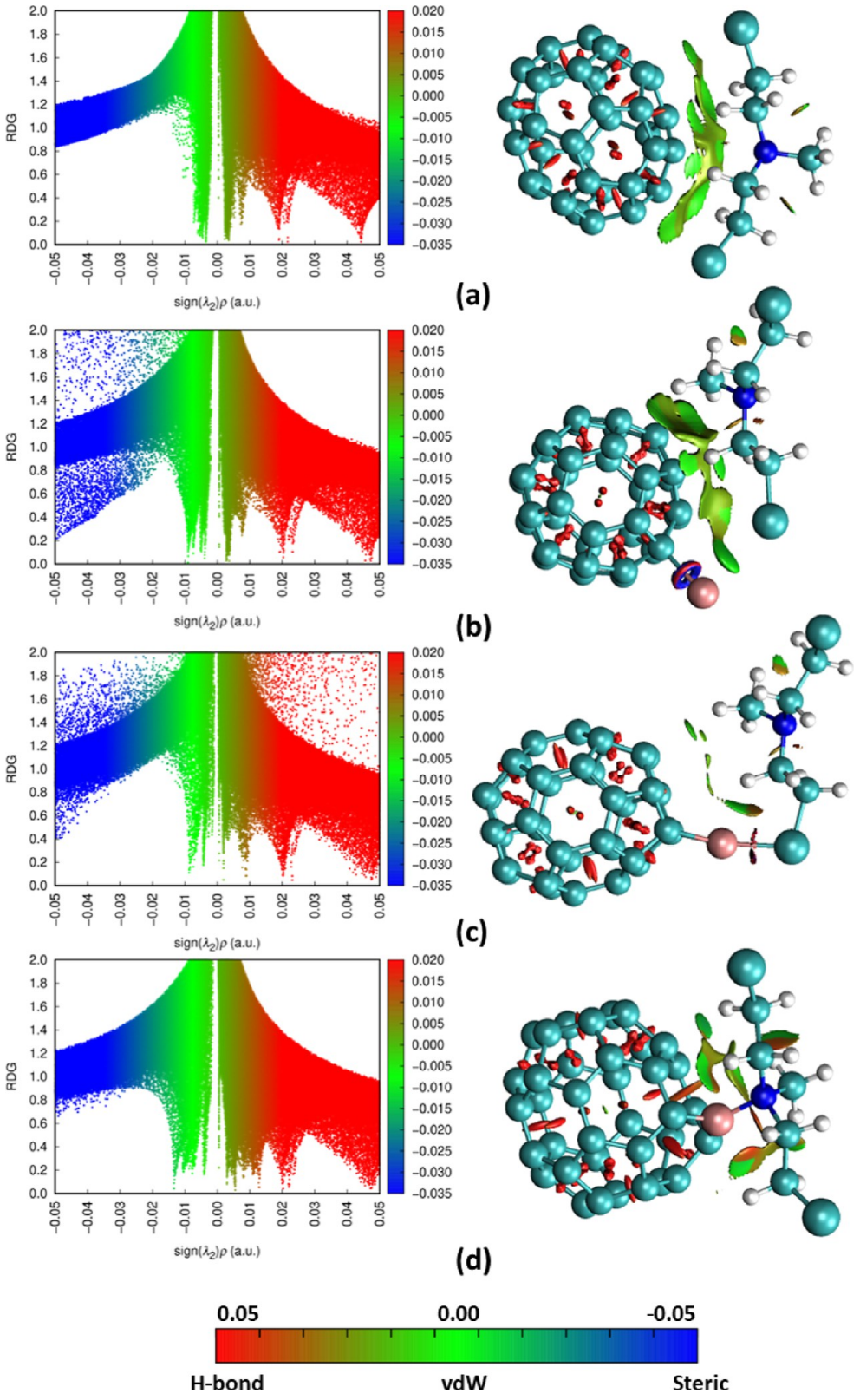

Figure 10. RDG scatter plots (left) and NCI isosurfaces (right) of (a) C_{36}/CHL, (b) Al−C_{36}/CHL, (c) Fe−C_{36}/CHL, and (d) B−C_{36}/CHL, respectively.

change in the energy gap (E_G) upon adsorption of CHL onto these fullerenes.

While the HOMO−LUMO gap is often cited as a key parameter for determining the electronic properties of molecular systems, including their potential for drug delivery or sensor applications, its interpretation as a standalone measure can be oversimplified. The HOMO−LUMO gap is related to the stability and reactivity of a molecule, but it does not fully capture the complexities of adsorption processes or sensor efficiency, which are influenced by a range of other

https://doi.org/10.1021/acsomega.4c08490
ACS Omega 2024, 9, 49786−49803

Table 5. Calculated Difference in E_G (ΔE_G), Recovery Time (τ), and Sensing Response (S) for CHL over C_{36}, Al−C_{36}, Fe−C_{36}, and B−C_{36} Fullerene, Respectively (T = 300 K)

complex	ΔE_G (eV)	t (sec)	S
C_{36}/CHL	−0.00136	6.55×10^{-9}	0.05409
Al−C_{36}/CHL	-0.03429^{α}	2.01×10^{-8}	2.7711^{α}
	-0.01959^{β}		1.13506^{β}
Fe−C_{36}/CHL	−0.00490	5.20×10^{9}	0.20889
B C_{36}/CHL	-0.17388^{α}	1.74×10^{16}	837.5223^{α}
	-0.30857^{β}		154243.3^{β}

factors, including charge transfer dynamics, molecular orientation, and interaction energies.[64] Eq 6, expresses the sensing response (S) as a function of the change in the HOMO−LUMO gap (ΔE_G) due to the interaction between the adsorbate (drug molecule) and the adsorbent (fullerene nanostructure). When the adsorption of the drug significantly alters the HOMO−LUMO gap, this corresponds to a notable change in conductivity, thereby enhancing the sensitivity of the sensor. This change can produce a detectable electrochemical signal, which confirms the adsorption process and facilitates drug detection.[65] However, it is important to acknowledge the limitations of using the HOMO−LUMO gap alone as a predictive measure of sensor efficiency. The gap reflects only the energy difference between the FMOs and does not account for all aspects of the electronic interaction between the drug and the nanostructure. For instance, the extent of charge transfer, the strength of the interaction (as measured by binding energies), and the nature of the adsorbate−adsorbent interface play equally important roles in determining the performance of sensor.[66−68]

3.8. Recovery Time. Recovery time has been demonstrated to be a crucial characteristic for chemical sensors that reflect the desorption process by heating the adsorbent to a higher temperature or by exposing it to UV light, and it is strongly correlated with the intensity of the contact. Higher interaction energies between molecules and an adsorbent lengthen the time it takes for them to recover and reduce their own interactions, which makes them less suitable for use in sensing applications. The following equation[17,64] yields the recovery time (τ).

$$\tau = \upsilon_0^{-1}\exp(-E_{ad}/\mathrm{KT}) \tag{7}$$

where T, K, and υ_0, respectively, stand for temperature, Boltzmann's constant, and the attempt frequency. Experimental evidence has shown that different photonic frequencies (υ_0) or thermal energy have been employed to cause the desorption of medicines and biomolecules.[64] Using a υ_0 of 10^{15} s^{-1}[64] and a temperature of 300 K, we predicted the recovery durations for the CHL from the chosen fullerene's perimeter (see Table 5). As mentioned, the recovery time is a key factor in determining the desorption rate of drug molecules from the sensor surface. The interaction energy between the drug molecules and the adsorbent (in this case, the fullerene variants) significantly affects the recovery time. A sensor with too strong an interaction may retain the drug molecule for a prolonged period, reducing the ability of the sensor to quickly reset for subsequent detections, thus diminishing its efficiency for real-time monitoring. On the other hand, a sensor with an interaction that is too weak may lead to insufficient sensitivity. Therefore, achieving an optimal balance in interaction energy is crucial for effective sensor design.[69] We discover that the shorter recovery times for the CHL drug molecule is 6.55×10^{-9} and 2.01×10^{-8} s, which is consistent with predictions given the substantial weak physisorption nature of pristine C_{36} and Al−C_{36} fullerenes, respectively. The pristine C_{36} and Al−C_{36} fullerenes, characterized by shorter recovery times and weaker physisorption with the CHL drug molecule, appear to be promising candidates for gas-phase drug sensor applications. Conversely, the strong chemical interaction between the CHL drug molecule and B−C_{36} or Fe−C_{36} fullerenes suggests their potential use in gas-phase drug delivery systems.[42,64,70]

3.9. Global Indices. In an effort to learn more about the reactivity of fullerenes or biomolecular systems, we have computed global indices such as electrophilicity (ω), chemical potential (μ), and chemical hardness (η). These global indices are computed with the use of the formulas found in refs 69 and 71.

$$\text{Chemical Potential } (\mu) = -(I + A)/2 \tag{8}$$

$$\text{Hardness } (\eta) = (I - A)/2 \tag{9}$$

$$\text{Electrophilicity } (\omega) = \frac{\mu^2}{2\eta} \tag{10}$$

where $I = -E_{HOMO}$ and $A = -E_{LUMO}$, Table 6 presents the calculated global indices using eq 8 through eq 10. A higher value of global hardness (η) indicates greater stability, which is closely related to the chemical robustness of the molecules. In this comparison, B−C_{36} and Al−C_{36} fullerenes emerge as the most stable, with the Al−C_{36}/CHL complex also demonstrating exceptional robustness. While CHL adsorption on C_{36} and Fe−C_{36} fullerenes shows minimal impact, significant changes in η are observed following CHL adsorption on B−C_{36} and Al−C_{36} fullerenes, with increases of 9.14% and 1.72%, respectively. Upon adsorption of the CHL drug molecule onto the fullerenes, the HOMO and LUMO positions of the systems cause a notable shift in the chemical potential (μ). The μ values change by +0.63%, −15.40%$^{\alpha}$, +0.53%$^{\alpha}$, and −4.52% for CHL adsorbed on C_{36}, B−C_{36}, Al−C_{36}, and Fe−C_{36} fullerenes, respectively. The significant change in chemical potential observed in the CHL/B−C_{36} and CHL/Fe−C_{36} systems confirms their strong interaction. Electrophilicity (ω), a measure of the tendency to accept electrons from atoms or molecules, further characterizes this interaction. The electrophilicity (ω) values for pristine C_{36}, B−C_{36}, Al−C_{36}, and Fe−C_{36} fullerenes are 0.273, 0.481^{α}, 0.492^{α}, and 0.274 eV, respectively. Upon CHL adsorption, these values change by 0,

Table 6. Global Indices Parameter of Systems

system/complex	μ (eV)	η (eV)	S $(eV)^{-1}$	W (eV)
C_{36}	−4.601	0.547	0.914	0.273
Al−C_{36}	-4.297^{α}	0.984^{α}	0.508^{α}	0.492^{α}
	-4.415^{β}	0.987^{β}	0.507^{β}	0.490^{β}
Fe−C_{36}	−4.114	0.548	0.913	0.274
B−C_{36}	-4.433^{α}	0.962^{α}	0.520^{α}	0.481^{α}
	-4.542^{β}	0.987^{β}	0.506^{β}	0.493^{β}
C_{36}/CHL	−4.630	0.546	0.916	0.273
Al−C_{36}/CHL	-4.320^{α}	0.967^{α}	0.517^{α}	0.483^{α}
	-4.450^{β}	0.977^{β}	0.512^{β}	0.488^{β}
Fe−C_{36}/CHL	−3.928	0.550	0.909	0.275
B−C_{36}/CHL	-3.750^{α}	0.874^{α}	0.572^{α}	0.437^{α}
	-3.940^{β}	0.832^{β}	0.601^{β}	0.416^{β}

https://doi.org/10.1021/acsomega.4c08490
ACS Omega 2024, 9, 49786−49803

Table 7. Calculated Value of LUMO Energy (E_{LUMO}), HOMO Energy (E_{HOMO}), HOMO−LUMO Gap (E_G), Adsorption Energy (E_{ad}), Recovery Time (τ), and Sensing Response (S) for CHL Adsorbed C_{36}, Al−C_{36}, Fe−C_{36}, and B−C_{36} Fullerene with Solvent Effect, Respectively

complex	E_{LUMO} (eV)	E_{HOMO} (eV)	E_G (eV)	E_f (eV)	E_{ad} (kJ/mol)	E_{FR} (%)	E_{GR} (%)	D (nm)	τ (sec)	S
C_{36}/CHL	−3.974	−5.065	1.090	−4.520	−36.18	1.043	−0.273	0.361	1.29×10^{-9}	0.119
Al−C_{36}/CHL	−3.213$^{\alpha}$	−5.120$^{\alpha}$	1.910$^{\alpha}$	−4.169$^{\alpha}$	−36.08	0.114$^{\alpha}$	−1.029$^{\alpha}$	0.319	1.23×10^{-9}	1.105$^{\alpha}$
	−3.352$^{\beta}$	−5.251$^{\beta}$	1.898$^{\beta}$	−4.301$^{\beta}$		0.120$^{\beta}$	−0.399$^{\beta}$			0.330$^{\beta}$
Fe−C_{36}/CHL	−3.263	−4.448	1.184	−3.856	−57.69	1.649	−1.981	0.237	5.5×10^{-6}	1.453
B−C_{36}/CHL	−2.979$^{\alpha}$	−4.640$^{\alpha}$	1.660$^{\alpha}$	−3.810$^{\alpha}$	−225.57	−11.790$^{\alpha}$	−13.68$^{\alpha}$	0.156	1.10×10^{23}	19117.14$^{\alpha}$
	−3.218$^{\beta}$	−4.782$^{\beta}$	1.563$^{\beta}$	−4.000$^{\beta}$		−9.718$^{\beta}$	−20.79$^{\beta}$			$4.8 \times 10^{6\beta}$

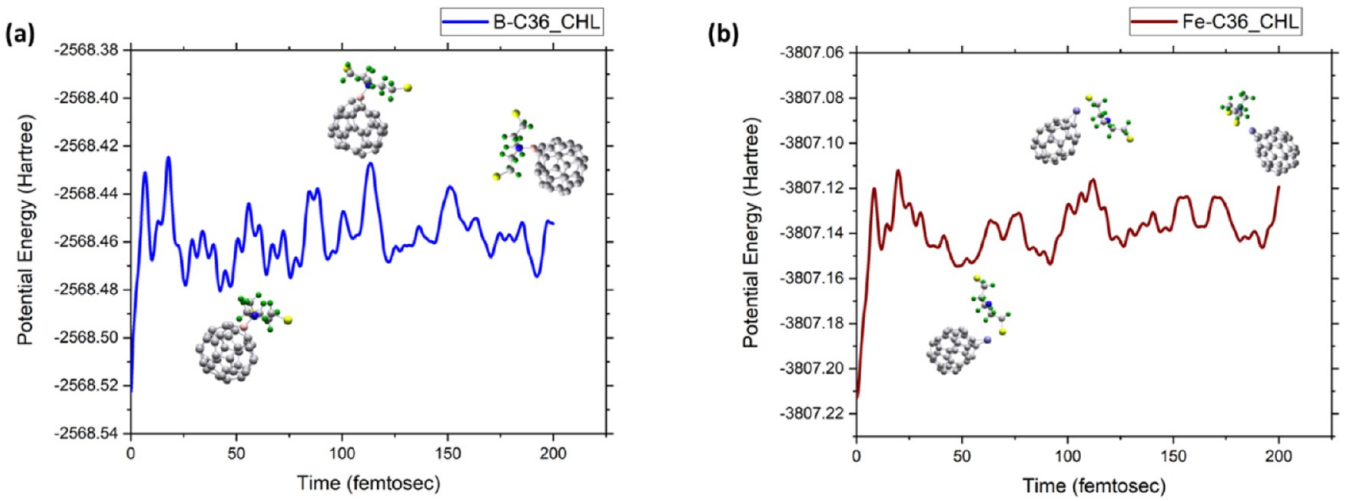

Figure 11. ADMP molecular dynamic profile of the PES for (a) B−C_{36}/CHL and (b) Fe−C_{36}/CHL system.

−9.15$^{\alpha}$ %, −1.83$^{\alpha}$ %, and +0.365%. The most significant alteration, observed with CHL adsorption on B−C_{36} fullerene, highlights their strong interaction.

3.10. Solvent Effect. In this study, the polarizable continuum model (PCM) approach has been utilized to assess the impact of the solvent[72] in DFT calculations, given that drug molecules are naturally present in biological environments. The complex interactions between drug molecules, solvent molecules, and carrier surfaces significantly affect binding affinities, sensing mechanisms, recovery times, and conformational changes.[73] We reoptimized each of the four fullerenes, the CHL drug molecule individually, and all the minimum configurations of CHL-fullerene complexes in an aqueous solvent using the DFT/B3LYP/6-31G(d,p) method with Grimme's D3 dispersion correction. The calculated adsorption energies, sensing responses, and recovery times are listed in Table 7. According to the electronic structures, the changes in E_G for CHL-adsorbed B−C_{36}, Al−C_{36}, and Fe−C_{36} fullerenes in water are 0.08, 0.023, and 0.085 eV, respectively, compared to the gas phase. Consequently, the sensing responses of B−C_{36}, Al−C_{36}, and Fe−C_{36} fullerenes to CHL shift from 837.5223$^{\alpha}$, 2.7711, and 0.20889 in the gas phase to 26554.87$^{\alpha}$, 1.15767$^{\alpha}$, and 1.52704 in water, respectively. This indicates that these fullerenes are sensitive to the drug molecule in a solvent medium. In the solvent effect, however, C_{36}/CHL are less interacting because of their similarly poor sensing responses of 0.122. Additionally, the results show that the B−C_{36}/CHL and Fe−C_{36}/CHL complexes had adsorption energies of −225.57 and −57.69 kJ/mol, respectively, in the aqueous phase. The adsorption energy of B−C_{36} fullerene with CHL is increased in an aqueous environment, leading to a longer recovery time in water. Due to this strong chemical interaction, B−C_{36} fullerene shows potential as a drug delivery system for the CHL anticancer drug in aquatic settings.[64] Moreover, as eq 6 shows, the recovery period decreases as the temperature rises during chemotherapy. However, the desorption process is made more difficult by the strong interactions that occur between the drug and fullerene. So, one of the most important factors for drug sensors is the degree of interaction between the drug and fullerene. A longer recovery time can be anticipated using eq 6 if the adsorption energy increases in a negative direction. The estimated recovery time at 300 K temperature is 5.5×10^{-6} s for a moderate contact and a minimum interatomic distance between the CHL and Fe−C_{36} fullerene in water solution. Based on previous findings regarding recovery times for various fullerene/CHL nanostructure systems, Fe−C_{36} fullerene emerges as a viable drug sensor due to its intermediate recovery time, reduced interatomic distance, and superior sensing response compared to both pristine C_{36} and Al−C_{36} fullerenes. Additionally, the recovery time of Fe−C_{36} fullerene is optimally balanced, neither excessively high nor too low, ensuring that the desorption process is not hindered.[21,64,70] To further understand the interaction mechanism between CHL and MM-decorated C_{36} fullerene beyond the influence of water as a solvent, we also calculated the adsorption energy in the presence of DMSO[74] (see Section S7 in the Supporting Information). Our results indicate that the adsorption energy trend remains consistent in both solvent cases.

For sensor applications, rapid recovery time is critical, requiring weak physisorption between the drug molecule and the adsorbent.[31,42,64,69,70,75−77] In contrast, drug delivery

https://doi.org/10.1021/acsomega.4c08490
ACS Omega 2024, 9, 49786−49803

systems benefit from strong chemisorption, indicated by more negative adsorption energy values exceeding 1 eV.[42,64,76] In our study, B−C_{36} exhibits strong interaction energy (−2.338 eV or −225.57 kJ/mol) with CHL, aligning with literature suggesting its suitability for drug delivery.[31,64,70,76] Conversely, Fe−C_{36} demonstrates minimal recovery time (5.5×10^{-6} s), better sensing response, and optimal adsorption energy, making it ideal for sensor applications due to quick desorption and enhanced sensitivity.[42,64,69,77]

Furthermore, we compared the adsorption energy (E_{ad}) and interatomic distances (d) of CHL over pristine and MM-modified C_{36} fullerene with the previously published studies in order to assess the versatility of both compounds in terms of their sensing mechanism toward the CHL drug molecule (see Section S6 in Supporting Information).

3.11. AIMD Simulations. Our findings indicate that B−C_{36} and Fe−C_{36} fullerenes exhibit intriguing interactions with the CHL drug molecule in an aqueous environment, outperforming both pristine and Al-decorated C_{36} fullerenes. Consequently, B−C_{36} fullerene is suitable for drug delivery applications, while Fe−C_{36} fullerene proves effective as a drug sensor for CHL in water. To assess the impact of temperature on the interaction between the CHL drug and B−C_{36} and Fe−C_{36} fullerenes, as well as the structural stability of the resulting complex, AIMD simulations were conducted using the ADMP method for up to 200 fs (with a time step of 0.2 fs). These simulations were performed with the PCM method under room-temperature conditions (300 K). Figure 11a,b displays the ADMP molecular dynamics profiles, showing the analysis of the PES for B−C_{36}/CHL and Fe−C_{36}/CHL. The results reveal that the potential energy variations are minimal: ranging from 0.01 to 0.04 Hartree (0.27 to 1.08 eV) for B−C_{36}/CHL and from 0.01 to 0.03 Hartree (0.27 to 0.82 eV) for Fe−C_{36}/CHL. These deviations are considered quite small for both systems. Despite these observations, the distance between the two fragments in the complexes remains relatively constant. Furthermore, for the B−C_{36}/CHL complex, the bond length between the N (CHL) and B (B−C_{36}) atoms changes from 1.56 Å in the ground state to 1.62 Å at 100 fs, 1.1628 Å at 150 fs, and 1.58 Å at 200 fs. In addition, in the case of the Fe−C_{36}/CHL complex, the bond length between the Cl (CHL) and Fe (Fe−C_{36}) atoms varies from 2.37 Å in the ground state to 2.38 Å at 100 fs, 2.65 Å at 150 fs, and 2.59 Å at 200 fs. The AIMD data show that no bonds are breaking or forming. The fact that the structure remains stable despite temperature changes suggest that electrostatic interactions are powerful enough to keep the pieces cohesive.

To assess the thermal stability of the CHL/B−C_{36} and CHL/Fe−C_{36} systems at different temperatures, we conducted AIMD simulations at 310 K. The results confirmed that both systems remain stable at this elevated temperature. The corresponding AIMD graphs are provided in the Supporting Information (Section S8).

4. CONCLUSIONS

In this study, the DFT-D3 method, applied to both gas and solvent phases, was used to investigate the adsorption process of the CHL drug molecule on C_{36}, Al−C_{36}, Fe−C_{36}, and B−C_{36} fullerenes. The results indicate that due to the solvent effect the adsorption energy of CHL with B−C_{36} is significantly higher in the aqueous phase compared to the gas phase. This increased reactivity and stability in water suggest that B−C_{36} fullerene is a promising candidate for drug delivery applications, particularly for the CHL anticancer drug. Conversely, the adsorption energy for the CHL drug molecule on Fe−C_{36} decreases in the presence of the solvent, leading to intermediate physisorption. Given its minimal recovery time, superior sensing response, intermediate physisorption, and reduced interatomic distance compared to C_{36} and Al−C_{36} fullerenes, Fe−C_{36} fullerene is well-suited for use as a drug sensor for CHL. AIMD simulations reveal that the B−C_{36}/CHL and Fe−C_{36}/CHL complexes are well-equilibrated and highly stable in the aqueous phase at 300 and 310 K respectively. These results show no bond breakage or formation. The observed structural stability despite temperature variations suggests that the electrostatic interactions are sufficiently strong to preserve the cohesion of the fragments. In conclusion, based on the combined findings from DFT and MD simulations, B−C_{36} and Fe−C_{36} fullerenes emerge as suitable candidates for specific applications. B−C_{36} fullerene is identified as a promising carrier for drug delivery, while Fe−C_{36} fullerene is well-suited as a drug sensor for the CHL anticancer drug.

■ ASSOCIATED CONTENT

Supporting Information

The Supporting Information is available free of charge at https://pubs.acs.org/doi/10.1021/acsomega.4c08490.

BSSE correction, adsorption performance with different basis set and method, adsorption energies (E_{ad}) with zero-point energy, ESP mapping after adsorption process, IR spectra analysis after adsorption, comparison table based on the adsorption, adsorption energy with effect of DMSO solvent, AIMD simulations at 310 K, and Cartesian coordinates of optimized structures (PDF)

■ AUTHOR INFORMATION

Corresponding Authors

Adisak Boonchun − *Department of Physics, Faculty of Science, Kasetsart University, Bangkok 10900, Thailand;* orcid.org/0000-0001-6527-4537; Email: adisak.bo@ku.th

Prafulla K. Jha − *Department of Physics, Faculty of Science, The Maharaja Sayajirao University of Baroda, Vadodara, Gujarat 39002, India;* orcid.org/0000-0002-9358-3940; Email: prafullaj@yahoo.com

Authors

Sourav Kanti Jana − *Department of Physics, Faculty of Science, Kasetsart University, Bangkok 10900, Thailand*

Namrata A. Tukadiya − *Department of Physics, Faculty of Science, The Maharaja Sayajirao University of Baroda, Vadodara, Gujarat 39002, India*

Complete contact information is available at: https://pubs.acs.org/10.1021/acsomega.4c08490

Notes

The authors declare no competing financial interest.

■ ACKNOWLEDGMENTS

A.B. is supported by the Kasetsart University Research and Development Institute, KURDI FF(KU-SRIU)7.67. S.K.J. greatly acknowledges for the Postdoctoral Fellowship from the Kasetsart University. We wish to thank NSTDA Super-

computer Center (ThaiSC) for providing computing resources for this work.

REFERENCES

(1) Allemand, P. M.; Khemani, K. C.; Koch, A.; Wudl, F.; Holczer, K.; Donovan, S.; Grüner, G.; Thompson, J. Organic Molecular Soft Ferromagnetism in a Fullerene C60. *Science* **1991**, *253* (5017), 301−302.
(2) Kroto, H. Space, Stars, C_{60}, and Soot. *Science* **1988**, *242* (4882), 1139−1145.
(3) López, A. M.; et al. Materials Chemistry of Fullerene C_{60} Derivatives. *J. Mater. Chem.* **2011**, *10*, 1305−1318.
(4) Celaya, C. A.; Hernández-Ayala, L. F.; Buendía Zamudio, F.; Vargas, J. A.; Reina, M. Adsorption of Melphalan Anticancer Drug on C24, B12N12, B12C6N6, B6C12N12 and B6C6N12 Nanocages: A Comparative DFT Study. *J. Mol. Liq.* **2021**, *329*, 115528.
(5) Jana, S. K.; Chodvadiya, D.; Som, N. N.; Jha, P. K. A Quantum Mechanical Prediction of C24 Fullerene as a DNA Nucleobase Biosensor. *Diamond Relat. Mater.* **2022**, *129* (June), 109305.
(6) Xiao, F.; Chen, Z.; Wei, Z.; Tian, L. Hydrophobic Interaction: A Promising Driving Force for the Biomedical Applications of Nucleic Acids. *Adv. Sci.* **2020**, *7* (16), 2001048.
(7) Anusha, T.; Bhavani, K. S.; Kumar, J. S.; Brahman, P. K. Designing and Fabrication of Electrochemical Nanosensor Employing Fullerene-C60 and Bimetallic Nanoparticles Composite Film for the Detection of Vitamin D3 in Blood Samples. *Diamond Relat. Mater.* **2020**, *104* (December 2019), 107761.
(8) Rather, J. A.; Al Harthi, A. J.; Khudaish, E. A.; Qurashi, A.; Munam, A.; Kannan, P. An Electrochemical Sensor Based on Fullerene Nanorods for the Detection of Paraben, an Endocrine Disruptor. *Anal. Methods* **2016**, *8* (28), 5690−5700.
(9) Goyal, R. N.; Gupta, V. K.; Bachheti, N.; Sharma, R. A. Electrochemical Sensor for the Determination of Dopamine in Presence of High Concentration of Ascorbic Acid Using a Fullerene-C60 Coated Gold Electrode. *Electroanalysis* **2008**, *20* (7), 757−764.
(10) Palanisamy, S.; Thirumalraj, B.; Chen, S. M.; Ali, M. A.; Al-Hemaid, F. M. A. Palladium Nanoparticles Decorated on Activated Fullerene Modified Screen Printed Carbon Electrode for Enhanced Electrochemical Sensing of Dopamine. *J. Colloid Interface Sci.* **2015**, *448*, 251−256.
(11) Hosseinian, A.; Vessally, E.; Yahyaei, S.; Edjlali, L.; Bekhradnia, A. A Density Functional Theory Study on the Interaction Between 5-Fluorouracil Drug and C24 Fullerene. *J. Cluster Sci.* **2017**, *28* (5), 2681−2692.
(12) Rad, A. S.; Aghaei, S. M.; Aali, E.; Peyravi, M. Study on the Electronic Structure of Cr- and Ni-Doped Fullerenes upon Adsorption of Adenine: A Comprehensive DFT Calculation. *Diamond Relat. Mater.* **2017**, *77* (May), 116−121.
(13) Li, W.; Zhao, T. Hydroxyurea Anticancer Drug Adsorption on the Pristine and Doped C70 Fullerene as Potential Carriers for Drug Delivery. *J. Mol. Liq.* **2021**, *340*, 117226.
(14) Shetti, N. P.; Malode, S. J.; Nandibewoor, S. T. Electrochemical Behavior of an Antiviral Drug Acyclovir at Fullerene-C60-Modified Glassy Carbon Electrode. *Bioelectrochemistry* **2012**, *88*, 76−83.
(15) Lyon, D. Y.; Adams, L. K.; Falkner, J. C.; Alvarez, P. J. J. Antibacterial Activity of Fullerene Water Suspensions: Effects of Preparation Method and Particle Size. *Environ. Sci. Technol.* **2006**, *40* (14), 4360−4366.
(16) Kanti Jana, S.; Som, N. N.; Jha, P. K. Theoretical Appraisements on the Interaction Behaviour of Amphetamine, Ketamine and Mercaptopurine Drug Molecules over C24 Fullerene: A Combined Dispersion Corrected DFT and MD Simulation Study. *J. Mol. Liq.* **2023**, *383* (May), 122084.
(17) Tukadiya, N. A.; Jana, S. K.; Chakraborty, B.; Jha, P. K. C24 Fullerene and Its Derivatives as a Viable Glucose Sensor: DFT and TD-DFT Studies. *Surf. Interfaces* **2023**, *41* (April), 103220.
(18) Jana, S. K.; Som, N. N.; Jha, P. K. Size-Dependent Fullerenes for Enhanced Interaction of l-Leucine: A Combined DFT and MD Simulations Approach. *Langmuir* **2024**, *40*, 13844.
(19) Liang, C.; Yang, J.; Hao, C.; Li, S.; Li, Y.; Jin, Y. The Interaction between Oxygen Atom and C 36 (D 6 H). *J. Mol. Struct.:THEOCHEM* **2008**, *851*, 342−347.
(20) Naderi, F.; Rostamian, S.; Naderi, B. A Study on the Electronic and Structural Properties of Fullerene C 36 and It's Interaction with Amino Acid. *Int. J. Math., Phys. Eng. Sci.* **2012**, *7* (13), 2006−2009.
(21) Reina, M.; Celaya, C. A.; Muñiz, J. C36 and C35E (E = N and B) Fullerenes as Potential Nanovehicles for Neuroprotective Drugs: A Comparative DFT Study. *ChemistrySelect* **2021**, *6* (19), 4844−4858.
(22) Lenik, J.; Wardak, C. Characteristic of a New Sensor for Indomethacin Determination. *Procedia Eng.* **2012**, *47*, 144−147.
(23) Li, X.; Du, P.; Zhang, W.; Zhang, L. Wastewater: A New Resource for the War against Illicit Drugs. *Curr. Opin. Environ. Sci. Health.* **2019**, *9*, 73−76.
(24) Merz, F. United Nations Office on Drugs and Crime: World Drug Report 2017. *Z. Strateg. Anal.* **2018**, *2*, 85−86.
(25) Ibrahim, M. A. A.; Rady, A.; Mandarawe, A. M. A.; Mohamed, L. A.; Shawky, A. M.; Hasanin, T. H. A.; Sidhom, P. A.; Soliman, M. E. S.; Moussa, N. A. M.; Moussa, N. A. M. Adsorption of Chlormethine Anti-Cancer Drug on Pure and Aluminum-Doped Boron Nitride Nanocarriers: A Comparative DFT Study. *Pharmaceuticals* **2022**, *15* (10), 1181.
(26) Rakib Hossain, M.; Mehade Hasan, M.; Ud Daula Shamim, S.; Ferdous, T.; Abul Hossain, M.; Ahmed, F. First-Principles Study of the Adsorption of Chlormethine Anticancer Drug on C24, B12N12 and B12C6N6 Nanocages. *Comput. Theor. Chem.* **2021**, *1197* (January), 113156.
(27) Hossain, M. R.; Hasan, M. M.; Nishat, M.; Noor-E-Ashrafi; Ahmed, F.; Ferdous, T.; Hossain, M. A. DFT and QTAIM Investigations of the Adsorption of Chlormethine Anticancer Drug on the Exterior Surface of Pristine and Transition Metal Functionalized Boron Nitride Fullerene. *J. Mol. Liq.* **2021**, *323*, 114627.
(28) Gholami, R.; Solimannejad, M. Potential of B24O24 Nanocluster for Sensing and Delivering Chlormethine Anticancer Drug: A DFT Study. *J. Mol. Model.* **2022**, *28* (8), 235.
(29) Mullett, W. M. Determination of Drugs in Biological Fluids by Direct Injection of Samples for Liquid-Chromatographic Analysis. *J. Biochem. Biophys. Methods* **2007**, *70* (2), 263−273.
(30) Ahmadi, R. Computational Study of the Fullerene Effects on the Properties of 16 Different Drugs: A Review. *Int. J. Nano Dimens.* **2018**, *9* (4), 325−335.
(31) Bibi, S.; Ur-Rehman, S.; Khalid, L.; Bhatti, I. A.; Bhatti, H. N.; Iqbal, J.; Bai, F. Q.; Zhang, H. X. Investigation of the Adsorption Properties of Gemcitabine Anticancer Drug with Metal-Doped Boron Nitride Fullerenes as a Drug-Delivery Carrier: A DFT Study. *RSC Adv.* **2022**, *12* (5), 2873−2887.
(32) Chen, K. Y.; Wu, S. Y.; Chen, H. T. Unraveling Catalytic Mechanisms for CO Oxidation on Boron-Doped Fullerene: A Computational Study. *ACS Omega* **2020**, *5* (44), 28870−28876.
(33) Sood, P.; Kim, K. C.; Jang, S. S. Electrochemical Properties of Boron-Doped Fullerene Derivatives for Lithium-Ion Battery Applications. *ChemPhysChem* **2018**, *19* (6), 753−758.
(34) Bilge, M. A. Dft Investigation of the Interaction of B- And Al-Doped C60 Fullerenes with Cyclopropylpipezarine. *J. Struct. Chem.* **2018**, *59* (6), 1271−1275.
(35) Li, J. L.; Yang, G. W. Iron Endohedral-Doped Boron Fullerene: A Potential Single Molecular Device with Tunable Electronic and Magnetic Properties. *J. Phys. Chem. C* **2009**, *113* (42), 18292−18295.
(36) Schlegel, H. B.; Iyengar, S. S.; Li, X.; Millam, J. M.; Voth, G. A.; Scuseria, G. E.; Frisch, M. J. Ab Initio Molecular Dynamics: Propagating the Density Matrix with Gaussian Orbitals. III. Comparison with Born-Oppenheimer Dynamics. *J. Chem. Phys.* **2002**, *117* (19), 8694−8704.
(37) Iyengar, S. S.; Schlegel, H. B.; Millam, J. M.; A Voth, G.; Scuseria, G. E.; Frisch, M. J. Ab Initio Molecular Dynamics: Propagating the Density Matrix with Gaussian Orbitals. II. Generalizations Based on Mass-Weighting, Idempotency, Energy Conservation and Choice of Initial Conditions. *J. Chem. Phys.* **2001**, *115* (22), 10291−10302.

https://doi.org/10.1021/acsomega.4c08490
ACS Omega 2024, 9, 49786−49803

(38) Foresman, J. B. *Exploring Chemistry with Electronic Structure Methods*, 2nd ed.; Gaussian Inc: Pittsburgh, PA, 1996.
(39) Zubair, H.; Mahmood, R. F.; Waqas, M.; Ishtiaq, M.; Iqbal, J.; Ibrahim, M. A. A.; Sayed, S. R. M.; Noor, S.; Khera, R. A. Effect of Tailoring π-Linkers with Extended Conjugation on the SJ-IC Molecule for Achieving High VOC and Improved Charge Mobility towards Enhanced Photovoltaic Applications. *RSC Adv.* **2023**, *13* (37), 26050−26068.
(40) Akram, M.; Siddique, S. A.; Iqbal, J.; Hussain, R.; Mehboob, M. Y.; Siddique, M. B. A.; Naveed, S.; Ali, B.; Hanif, A.; Sajid, M.; Shoukat, S. End-Capped Engineering of Bipolar Diketopyrrolopyrrole Based Small Electron Acceptor Molecules for High Performance Organic Solar Cells. *Comput. Theor. Chem.* **2021**, *1201* (February), 113242.
(41) Sheikhi, M.; Kaviani, S.; Azarakhshi, F.; Shahab, S. Superalkali X3O (X = Li, Na, K) Doped B12N12 Nano-Cages as a New Drug Delivery Platform for Chlormethine: A DFT Approach. *Comput. Theor. Chem.* **2022**, *1212* (April), 113722.
(42) Kaviani, S.; Izadyar, M. First-Principles Study of the Binding Affinity of Monolayer BC6N Nanosheet: Implications for Drug Delivery. *Mater. Chem. Phys.* **2022**, *276* (October 2021), 125375.
(43) Zhang, N.; Luo, J.; Blowers, P.; Farrell, J. Understanding Trichloroethylene Chemisorption to Iron Surfaces Using Density Functional Theory. *Environ. Sci. Technol.* **2008**, *42* (6), 2015−2020.
(44) Peljhan, S.; Kokalj, A. DFT Study of Gas-Phase Adsorption of Benzotriazole on Cu(111), Cu(100), Cu(110), and Low Coordinated Defects Thereon. *Phys. Chem. Chem. Phys.* **2011**, *13* (45), 20408−20417.
(45) Sherrill, C. D. *Counterpoise Correction and Basis Set Superposition Error*; Self-Published, 2010; pp 1−5.
(46) Chai, J. Da; Head-Gordon, M. Long-Range Corrected Hybrid Density Functionals with Damped Atom-Atom Dispersion Corrections. *Phys. Chem. Chem. Phys.* **2008**, *10* (44), 6615−6620.
(47) Adjizian, J. J.; Vlandas, A.; Rio, J.; Charlier, J. C.; Ewels, C. P. Ab Initio Infrared Vibrational Modes for Neutral and Charged Small Fullerenes (C20, C24, C26, C28, C30 and C60). *Philos. Trans. R. Soc., A* **2016**, *374*, 20150323.
(48) Chandiramouli, R.; Srivastava, A.; Nagarajan, V. NO Adsorption Studies on Silicene Nanosheet: DFT Investigation. *Appl. Surf. Sci.* **2015**, *351*, 662−672.
(49) Demir, S.; Fellah, M. F. A DFT Study on Pt Doped (4,0) SWCNT: CO Adsorption and Sensing. *Appl. Surf. Sci.* **2020**, *504*, 144141.
(50) Kaviani, S.; Izadyar, M.; Khavani, M.; Housaindokht, M. R. A Combined Molecular Dynamics and Quantum Mechanics Study on the Interaction of Fe3+ and Human Serum Albumin Relevant to Iron Overload Disease. *J. Mol. Liq.* **2020**, *317*, 113933.
(51) Zubatiuk, T.; Hill, G.; Leszczynska, D.; Fan, M.; Rony, A. H.; Leszczynski, J. Insight into Mechanism of Iron-Oxides Reduction in Atmospheres of CH4 and CO. *Chem. Phys. Lett.* **2018**, *706*, 708−714.
(52) Lu, T.; Chen, F. Multiwfn: A multifunctional wavefunction analyzer. *J. Comput. Chem.* **2012**, *33* (5), 580−592.
(53) Niu, X.; Huang, Z.; Ma, L.; Shen, T.; Guo, L. Density Functional Theory, Natural Bond Orbital and Quantum Theory of Atoms in Molecule Analyses on the Hydrogen Bonding Interactions in Tryptophan-Water Complexes. *J. Chem. Sci.* **2013**, *125* (4), 949−958.
(54) Kaviani, S.; Shahab, S.; Sheikhi, M. Adsorption of Alprazolam Drug on the B12N12 and Al12N12 Nano-Cages for Biological Applications: A DFT Study. *Phys. E* **2021**, *126*, 114473.
(55) Zaid, H. A-S.; Senturk Dalgic, F. K. Theoretical Study of the Adsorption of BMSF-BENZ Drug for Osteoporosis Disease Treatment on Al-Doped Carbon Nanotubes (Al-CNT) as a Drug Delivery Vehicle. *Eur. J. Chem.* **2021**, *12* (3), 114−322.
(56) Kanzariya, A.; Vadalkar, S.; Jana, S. K.; Saini, L. K.; Jha, P. K. An Ab-Initio Investigation of Transition Metal-Doped Graphene Quantum Dots for the Adsorption of Hazardous CO2, H2S, HCN, and CNCl Molecules. *J. Phys. Chem. Solids* **2024**, *186* (July 2023), 111799.
(57) Johnson, E. R.; Keinan, S.; Mori-Sánchez, P.; Contreras-García, J.; Cohen, A. J.; Yang, W. Revealing Noncovalent Interactions. *J. Am. Chem. Soc.* **2010**, *132* (18), 6498−6506.
(58) Kurban, M.; Muz, I. ·. Theoretical Investigation of the Adsorption Behaviors of Fluorouracil as an Anticancer Drug on Pristine and B-, Al-, Ga-Doped C36 Nanotube. *J. Mol. Liq.* **2020**, *309*, 113209.
(59) Ahmadi Peyghan, A.; Hadipour, N. L.; Bagheri, Z. Effects of Al Doping and Double-Antisite Defect on the Adsorption of HCN on a BC2N Nanotube: Density Functional Theory Studies. *J. Phys. Chem. C* **2013**, *117* (5), 2427−2432.
(60) Dipak, P.; Tiwari, D. C.; Samadhiya, A.; Kumar, N.; Biswajit, T.; Singh, P. A.; Tiwari, R. K. Synthesis of Polyaniline (Printable Nanoink) Gas Sensor for the Detection of Ammonia Gas. *J. Mater. Sci.:Mater. Electron.* **2020**, *31* (24), 22512−22521.
(61) Tiwari, D. C.; Atri, P.; Sharma, R. Sensitive Detection of Ammonia by Reduced Graphene Oxide/Polypyrrole Nanocomposites. *Synth. Met.* **2015**, *203*, 228−234.
(62) Illyaskutty, N.; Kohler, H.; Trautmann, T.; Schwotzer, M.; Pillai, V. P. M. Enhanced Ethanol Sensing Response from Nanostructured MoO3:ZnO Thin Films and Their Mechanism of Sensing. *J. Mater. Chem. C* **2013**, *1* (25), 3976−3984.
(63) Yang, Y.; Sun, A.; Eslami, M. A Density Functional Theory Study on Detection of Amphetamine Drug by Silicon Carbide Nanotubes. *Phys. E* **2021**, *125*, 114411.
(64) Rahman, H.; Hossain, M. R.; Ferdous, T. The Recent Advancement of Low-Dimensional Nanostructured Materials for Drug Delivery and Drug Sensing Application: A Brief Review. *J. Mol. Liq.* **2020**, *320*, 114427.
(65) Sun, X.; Wan, X.; Li, G.; Yu, J.; Vahabi, V. Amantadine Antiparkinsonian Drug Adsorption on the AlN and BN Nanoclusters: A Computational Study. *Phys. Lett. A: Gen. At. Solid State Phys.* **2020**, *384* (5), 126128.
(66) Ivanov, M. V.; Reid, S. A.; Rathore, R. Game of Frontier Orbitals: A View on the Rational Design of Novel Charge-Transfer Materials. *J. Phys. Chem. Lett.* **2018**, *9* (14), 3978−3986.
(67) McCarroll, M. E.; Shi, Y.; Harris, S.; Puli, S.; Kimaru, I.; Xu, R.; Wang, L.; Dyer, D. J. Computational Prediction and Experimental Evaluation of a Photoinduced Electron-Transfer Sensor. *J. Phys. Chem. B* **2006**, *110* (46), 22991−22994.
(68) Hoffmann, M. W. G.; Prades, J. D.; Mayrhofer, L.; Hernandez-Ramirez, F.; Järvi, T. T.; Moseler, M.; Waag, A.; Shen, H. Highly Selective SAM-Nanowire Hybrid NO2 Sensor: Insight into Charge Transfer Dynamics and Alignment of Frontier Molecular Orbitals. *Adv. Funct. Mater.* **2014**, *24* (5), 595−602.
(69) Hossain, M. A.; Hossain, M. R.; Hossain, M. K.; Khandaker, J. I.; Ahmed, F.; Ferdous, T.; Hossain, M. A. An Ab Initio Study of the B35 Boron Nanocluster for Application as Atmospheric Gas (NO,NO2,N2O,NH3) Sensor. *Chem. Phys. Lett.* **2020**, *754* (2), 137701.
(70) Nagarajan, V.; Chandiramouli, R. A Study on Quercetin and 5-Fluorouracil Drug Interaction on Graphyne Nanosheets and Solvent Effects—A First-Principles Study. *J. Mol. Liq.* **2019**, *275*, 713−722.
(71) Vadalkar, S.; Chodvadiya, D.; Som, N. N.; Vyas, K. N.; Jha, P. K.; Chakraborty, B. An Ab-Initio Study of the C18 Nanocluster for Hazardous Gas Sensor Application. *ChemistrySelect* **2022**, *7* (3), No. e202103874.
(72) Etminan, N.; Yoose, M.; Raissi, H.; Hakimi, M. Solvent Effects on the Stability and the Electronic Properties of Histidine/Pd-Doped Single-Walled Carbon Nanotube Biosensor. *J. Mol. Liq.* **2015**, *214*, 313.
(73) Cossi, M.; Barone, V.; Cammi, R.; Tomasi, J. Ab Initio Study of Solvated Molecules: A New Implementation of the Polarizable Continuum Model. *Chem. Phys. Lett.* **1996**, *255* (4−6), 327−335.
(74) Ignaczak, A. Solvent Effect on the Potential Energy Surfaces for the One-Electron Reduction of CF3X (X = Cl, Br, I) Molecules: A DFT PCM Study. *J. Phys. Chem. A* **2012**, *116* (47), 11694−11701.
(75) Saikia, U.; Saikia, N.; Waters, K.; Pandey, R.; Sahariah, M. B. Electronic Properties of Acetaminophen Adsorbed on 2D Clusters: A

https://doi.org/10.1021/acsomega.4c08490
ACS Omega 2024, 9, 49786−49803

First Principles Density Functional Study. *ChemistrySelect* **2017**, *2* (13), 3613−3621.
(76) Tamafo Fouegue, A. D.; de Paul Zoua, V.; Kounou, G. N.; Ndjopme Wandji, B. L.; Ghogomu, J. N.; Ntieche, R. A. DFT Investigation of Temozolomide Drug Delivery by Pure and Boron Doped C24 Fullerene-like Nanocages. *Nanoscale Adv.* **2023**, *5* (21), 5880−5891.
(77) Salem-Bekhit, M. M.; Da'i, M.; Rakhmatullaeva, M. M.; Mirzaei, M.; Al Zahrani, S.; Alhabib, N. A. The Drug Delivery of Methimazole through the Sensing Function Assessments of BeO Fullerene-like Particles: DFT Study. *Chem. Phys. Impact* **2023**, *7* (September), 100335.

https://doi.org/10.1021/acsomega.4c08490
ACS Omega 2024, 9, 49786−49803